INFECTIOUS DISEASES

Antibody cocktails based on the occupationally acquired immunity of pediatricians neutralize and confer protection against RSV and hMPV

Hui Zhai[1,2]†, Wenxiang Yu[3,4]†, Jinyue Wang[3]†, Jie Deng[3,4]†, Siyu Lei[5,6,7], Teng Zhou[1,2], Yixin Li[3,4], Kaijun Xu[3,4], Mengyang Ma[3,4], Rui Feng[3], Yaling Hu[8], Luo Ren[1,2]*, Yunlong Cao[5,7,9]*, Enmei Liu[1,10]*, Xiangxi Wang[1,3,4,8,9]*

Human respiratory syncytial virus (RSV) and human metapneumovirus (hMPV) are major causes of severe respiratory infections in young children, older adults, and immunocompromised individuals. Here, we isolated RSV fusion (F) protein–specific B cells from pediatricians who are routinely exposed to these viruses. We then derived monoclonal antibodies (mAbs) from those B cells to characterize their binding and neutralization profiles. Among the isolated mAbs, we found that CNR2056 and CNR2053 (targeting site Ø of the pre–F protein) potently neutralized diverse RSV A and B strains; another mAb, CNR2047 (targeting site III), uniquely exhibited cross-neutralization capacity against both RSV and hMPV variants. In vivo, prophylactic administration of CNR2056 and CNR2053 controlled lung viral loads and pathology in RSV A2– and B9320-challenged cotton rats. Moreover, a prophylactic dose of 0.5 milligrams per kilogram of CNR2047 resulted in complete protection against hMPV in the lungs of BALB/c mice. Structural analysis revealed unique binding modes for the three mAbs, supporting the potential for rational mAb cocktail design. Deep mutational scanning for RSV F further demonstrated that mutations required to evade CNR2053 and CNR2056 were primarily in evolutionarily constrained sites, suggesting a fitness cost to immune escape. Rationally combining site Ø– and site III–directed mAbs (e.g., CNR2056-CNR2047) into cocktails conferred additive effects, expanding coverage to hMPV and minimizing risk of escape variants. Thus, rationally designed cocktails of CNR2056, CNR2053, and CNR2047 may offer a versatile immunoprophylactic agent against a range of pneumoviruses with potential to protect against both current and future variants.

INTRODUCTION

Human respiratory syncytial virus (RSV) and human metapneumovirus (hMPV), members of the Pneumoviridae family, represent major global health burdens, causing acute lower respiratory tract infection in older adults, immunocompromised individuals, and children aged ≤2 years, particularly infants under 6 months of age (*1*–*3*). RSV is the leading cause of lower respiratory tract infection, accounting for 30 to 50% of hospitalizations in children; human metapneumovirus (hMPV) follows closely, causing 6 to 15% of such hospitalizations and ranking as the second most prevalent pathogen (*4*–*7*). Despite recent US Food and Drug Administration–approved RSV vaccines for older adults using stabilized prefusion (pre-F) antigens (*8*), pediatric vaccine development faces challenges because of vaccine-enhanced respiratory disease risks (*9*). Furthermore, vaccination before immune-ablative therapies is often ineffective for immunocompromised individuals, indicative of an urgent need for effective alternatives to vaccination. Moreover, approved therapeutic or prophylactic options for hMPV infection are lacking. These highlight the critical unmet needs in this area.

The use of neutralizing monoclonal antibodies (mAbs) offers a highly effective alternative for protecting against viral infections. For both RSV and hMPV, the primary target for eliciting functional neutralizing antibodies is the fusion (F) protein located on the surfaces of virions, which plays a crucial role in mediating viral entry into host cells. As the F protein transitions from its metastable pre-F form to the stable postfusion (post-F) form, marked conformational changes occur, which initiate viral membrane fusion. Most potent neutralizing antibodies specifically target epitopes that are exclusively present on the pre-F form. Therefore, stabilized pre-F has been extensively used in the development of current vaccines and prophylactic antibodies (*10*–*12*). The RSV F protein contains six major antigenic sites (Ø to V), with pre-F–specific sites Ø and V eliciting the most potent neutralizing responses (*13*–*15*). However, high immune pressure on these sites drives viral escape; suptavumab (site V) failed in phase 3 trials because of resistant variants (*16*), whereas nirsevimab (site Ø) showed reduced efficacy against clinical isolates with site Ø mutations (*17*). In contrast, some site III/IV antibodies, such as RSV-199, M2D2, and 101F, have demonstrated broader neutralization across RSV subgroups and hMPV, but their neutralizing activities can vary considerably (*18*–*20*). Last, site I/II–targeting antibodies show limited efficacy, exemplified by the first approved RSV therapeutic, palivizumab (*21*).

Although RSV and hMPV exhibit slower evolutionary rates than influenza or coronaviruses (maintaining a single serotype with A/B subgroups showing ~5% F protein sequence divergence) (*22*, *23*),

[1]Department of Respiratory Medicine, Children's Hospital of Chongqing Medical University, National Clinical Research Center for Children and Adolescents' Health and Diseases, Ministry of Education Key Laboratory of Child Development and Disorders, Chongqing 400014, China. [2]Chongqing Key Laboratory of Child Rare Diseases in Infection and Immunity, Chongqing 400014, China. [3]State Key Laboratory of Biomacromolecules, Institute of Biophysics, Chinese Academy of Sciences, Beijing 100101, China. [4]University of Chinese Academy of Sciences, Beijing 100049, China. [5]Peking-Tsinghua Center for Life Sciences, Peking University, Beijing 100871, China. [6]Academy for Advanced Interdisciplinary Studies, Peking University, Beijing 100871, China. [7]Biomedical Pioneering Innovation Center (BIOPIC), School of Life Sciences, Peking University, Beijing 100871, China. [8]IBP-Sinovac Joint Laboratory of Cutting-edge Technologies and Vaccine & Drug Development, Beijing 100101, China. [9]Changping Laboratory, Beijing 102206, China. [10]Chongqing Medical University, Chongqing 400016, China.
†These authors contributed equally to this work.
*Corresponding author. Email: renluo@yeah.net (L.R.); yunlongcao@pku.edu.cn (Y.C.); emliu186@126.com (E.L.); xiangxi@ibp.ac.cn (X.W.)

surveillance data demonstrate that emerging genotypes periodically become dominant circulating strains (*24*). Of particular concern is the widespread deployment of RSV vaccines, which may accelerate the emergence of escape variants because of increased immune pressure (*25*), similar to observations made regarding severe acute respiratory syndrome coronavirus 2 (SARS-CoV-2) evolution (*26*). Although focusing antibody responses on conserved epitopes can mitigate escape risks, this strategy frequently comes at the cost of reduced neutralization potency. To address these challenges, we developed an integrated approach that began with isolating mAbs from pediatricians who experience repeated occupational exposure to these pneumoviruses. We performed detailed structural characterization of their binding modes and comprehensive deep mutational profiling of potential escape variants, supported by viral surveillance of real-world mutation frequency. These insights facilitated the rational design of antibody cocktails that strategically combine strain-specific and cross-reactive mAbs, which we tested as a prophylactic against RSV and hMPV in vivo.

RESULTS

Occupationally exposed pediatricians yield anti–pre-F mAbs that potently neutralize RSV and hMPV

We first established a cohort consisting of 10 pediatric health care workers who have worked in the Department of Respiratory Medicine at the Children's Hospital of Chongqing Medical University for more than 10 years and 14 healthy adults as controls. Serum neutralization assays revealed that RSV-specific neutralizing antibody titers in the repeatedly exposed group were more than threefold higher than those in the healthy controls without occupational exposure to RSV/hMPV, and three pediatricians with high neutralizing titers were selected for the following study (Fig. 1A and fig. S1A). Using purified RSV pre–F glycoprotein (DS-Cav1) (*13*) as a bait, we sorted specific memory B cells from the peripheral blood mononuclear cells (PBMCs) of these three individuals (fig. S1, B and C). Subsequently, we performed single-cell V(D)J sequencing (scVDJ-seq) with pre-F feature barcodes on antigen-specific memory B cells, extracted the productive heavy-light–chain paired V(D)J sequences, and expressed the antibodies in vitro as human IgG1.

Characterization by enzyme-linked immunosorbent assay (ELISA) revealed that 56 of the 57 mAbs demonstrated robust binding to RSV pre-F, with EC_{50} (median effective concentration) values ranging from 8 to 53 ng/ml (table S1). This finding confirms the integrity of our probe-based identification of RSV F–specific B cells. To map the epitopes targeted by these mAbs, each was tested for binding competition with a panel of five well-defined RSV F–specific antibodies. Using biolayer interferometry (BLI) competition profiles, structural validation, binding characteristics (pre-F–specific or cross-reactive to pre- and post-F), and germline gene usage (Fig. 1, B and C; fig. S1, D to F; and table S2), we clustered the expressed mAbs: 25 mAbs targeted site Ø, 3 bound to site II (antigenic site overlapping with III and V, but only site II mAbs were cross-reactive to pre- and post-F), 9 recognized site III (with identical *IGHV3-21*/*IGLV1-40* pairing), 7 directed to site IV, and 11 belonged to site V (mainly derived from *IGHV1-18/IGKV2-30* pairs) (Fig. 1D). All 57 mAbs exhibited detectable neutralization against at least one RSV strain, with 51 achieving a median inhibitory concentration (IC_{50}) value of less than 50 ng/ml and 25 achieving an IC_{50} of less than 10 ng/ml, as determined by indirect immunofluorescence assays (table S1). Site Ø–directed antibodies, exemplified by CNR2056 and CNR2053, showcased potent and unbiased neutralizing activities against four RSV A and B strains (Fig. 1C and table S1). CNR2047 exhibited broad and potent activity across RSV and hMPV subtypes (Fig. 1, E and F, and table S1). These mAbs also displayed high apparent affinities for binding to RSV pre-F or hMPV pre-F, correlating with somatic hypermutation (SHM) rates exceeding 10% in the heavy chain (V_H) (Fig. 1E and fig. S1, D to F), suggesting that repeated affinity maturation may have enhanced potency and cross-reactivity to hMPV.

Classic plaque reduction neutralization tests (PRNTs) further substantiated the potency of CNR2056 and CNR2053 against four RSV strains, with IC_{50} values ranging from 1.1 to 2.3 ng/ml and 1.1 to 5.1 ng/ml, respectively. In contrast, the IC_{50} values of positive controls MEDI8897 and MK-1654 ranged from 1.5 to 37.0 ng/ml and 6.4 to 23.3 ng/ml, respectively (Fig. 1F and table S1). CNR2047 also robustly neutralized hMPV, with IC_{50} values of 6.9 to 18.3 ng/ml (Fig. 1F). Collectively, these findings highlight that a subset of anti-F antibodies isolated from healthy pediatricians exhibits high potency and neutralizing breadth, positioning these antibodies as promising candidates for the development of next-generation immunoprophylactic agents against RSV and hMPV.

CNR2056 and CNR2053 confer prophylactic protection in cotton rats

To evaluate whether the enhanced neutralizing activities of CNR2056 and CNR2053 observed in vitro could translate into antiviral efficacy in vivo, we conducted prophylactic efficacy studies against RSV infection, using MEDI8897 as a positive control (Fig. 2A). Cotton rats were intramuscularly administered CNR2056, CNR2053, or MEDI8897 at one of six doses, ranging from 2 to 0.063 mg/kg, 1 day before challenge with RSV strains A2 or B9320. The negative control group received phosphate-buffered saline (PBS) (Fig. 2B). Lung tissues were harvested 4 days after challenge, with right lung samples used for viral titer assessment and left lung samples for histopathology scoring. All tested antibodies demonstrated dose-dependent protection, characterized by reduced viral titers or complete viral clearance (undetectable) in the lungs of infected cotton rats. MEDI8897 achieved this at a maximum dose of 2 mg/kg, whereas CNR2053 and CNR2056 enabled viral clearance at doses of 1 and 0.5 mg/kg, respectively (Fig. 2B). The calculated doses required to achieve 100- and 1000-fold reductions in viral titers in the lungs, compared with PBS-treated controls, were 0.27 and 0.46 mg/kg for CNR2053, 0.4 and 1.25 mg/kg for MEDI8897, and 0.28 and 0.93 mg/kg for CNR2056, respectively (Fig. 2B). In the B9320 challenge group, CNR2056 was estimated to achieve a 100-fold reduction in pulmonary viral titer at a theoretical dose of 0.2 mg/kg. In contrast, doses of 0.34 and 0.57 mg/kg were estimated to achieve a 100-fold reduction for CNR2053 and MEDI8897, respectively (Fig. 2B). An extremely low dose of 0.5 mg/kg of CNR2056 resulted in complete protection in the lungs from B9320 infection, whereas a dose of 2 mg/kg for MEDI8897 was required to achieve this (Fig. 2B). Histopathological analysis of the lungs revealed that all three antibodies effectively mitigated pulmonary inflammation induced by RSV infections in a dose-dependent manner (Fig. 2C and fig. S2). Animals receiving doses of CNR2053 or CNR2056 at $\geq$0.5 mg/kg exhibited minimal peribronchiolitis and interstitial inflammation, as indicated by significantly ($P < 0.05$) lower histology scores than those receiving the same dose of MEDI8897 in B9320 challenge

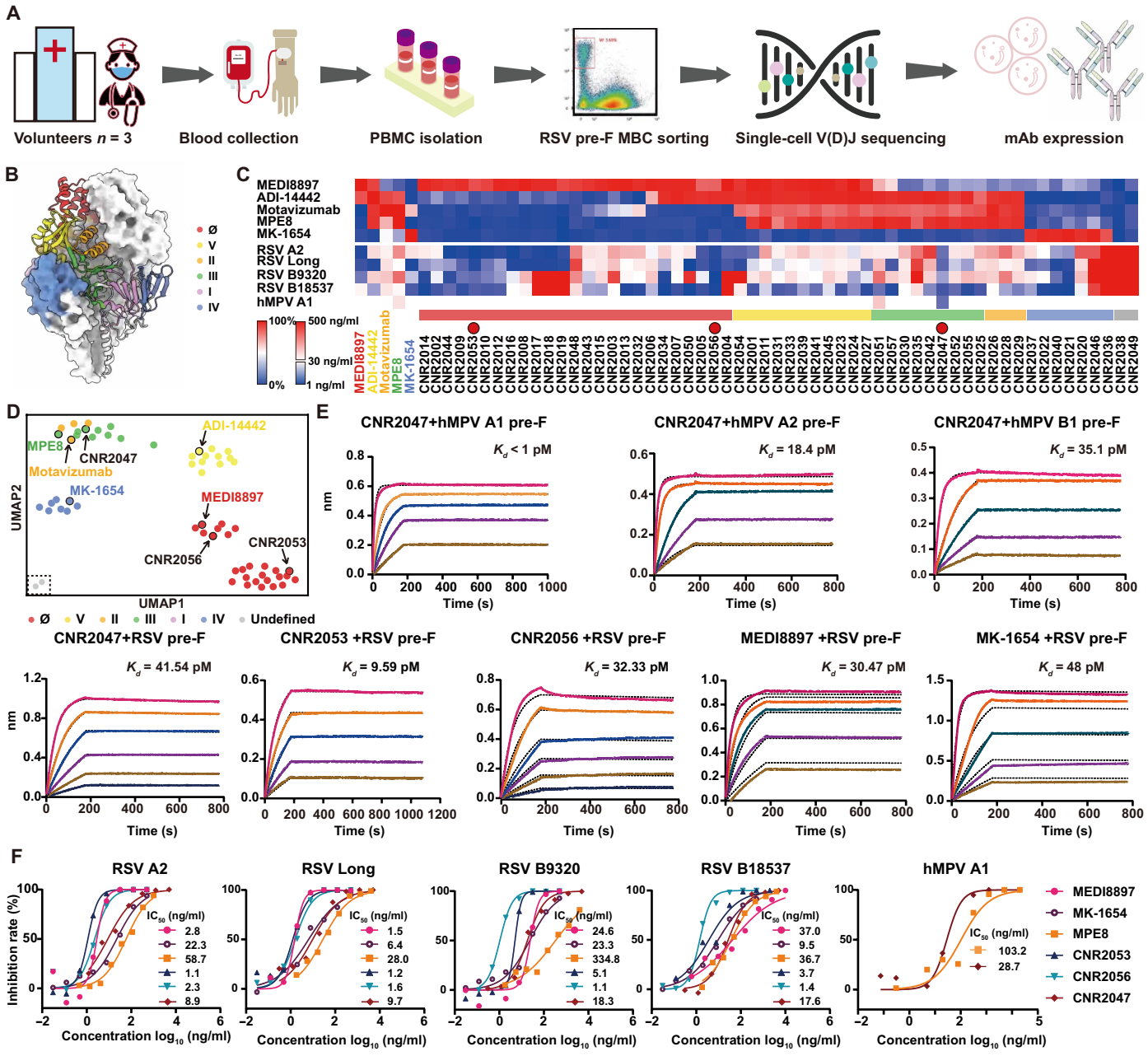

Fig. 1. Anti-F antibodies from healthy pediatricians neutralize RSV and hMPV. (**A**) Schematic diagram of the mAb identification process. (**B**) Schematic diagram of the defined epitopes of RSV pre-F. (**C**) Heatmap depicting inhibition rates (top) against RSV F antibodies with well-defined epitopes (MEDI8897, site Ø; motavizumab, site II; MPE8, site III; MK1654, site IV; and ADI-14442, site V) by competition assay and neutralizing activities (bottom) against RSV (A2, Long, B9320, and B18537) and hMPV A1 by indirect immunofluorescence assays. Red circles indicate the three antibodies (CNR2053, CNR2056, and CNR2047) selected from the initial screen of 57 antibodies for further functional characterization. (**D**) Uniform Manifold Approximation and Projection (UMAP) of RSV F protein–specific antibodies colored by epitope clusters. Each point represents a mAb, with colors indicating distinct epitope groups defined by combination with competitive binding assays, structural validations (four antigen-Fab complex structures in this manuscript), binding characteristics (pre-F–specific or cross-reactive to pre- and post-F), and germline gene usage. (**E**) Affinity measurements of CNR2053, CNR2056, and CNR2047 to purified recombinant RSV A2 and hMPV pre–F proteins using BLI, with K_d (equilibrium dissociation constant) values shown. (**F**) Dose-response regression curves for CNR2053, CNR2056, CNR2047, and positive control mAbs against RSV (A2, Long, B9320, and B18537) and hMPV A1, determined by the PRNT. IC_{50} values represent the concentrations of mAbs required to reduce viral infection by 50%.

groups, although pathology was comparable in the A2 challenge groups (Fig. 2, C and D). MEDI8897 administration resulted in moderate peribronchiolitis at doses of ≥0.5 mg/kg, with lower doses leading to more severe peribronchiolitis and substantial inflammatory cell infiltration in the RSV B9320 challenge group (Fig. 2C and fig. S2). No evidence of enhanced respiratory disease was observed, even at the lowest administered dose of 0.063 mg/kg (Fig. 2, C and D). To further explore the potential of CNR2053 and CNR2056 as

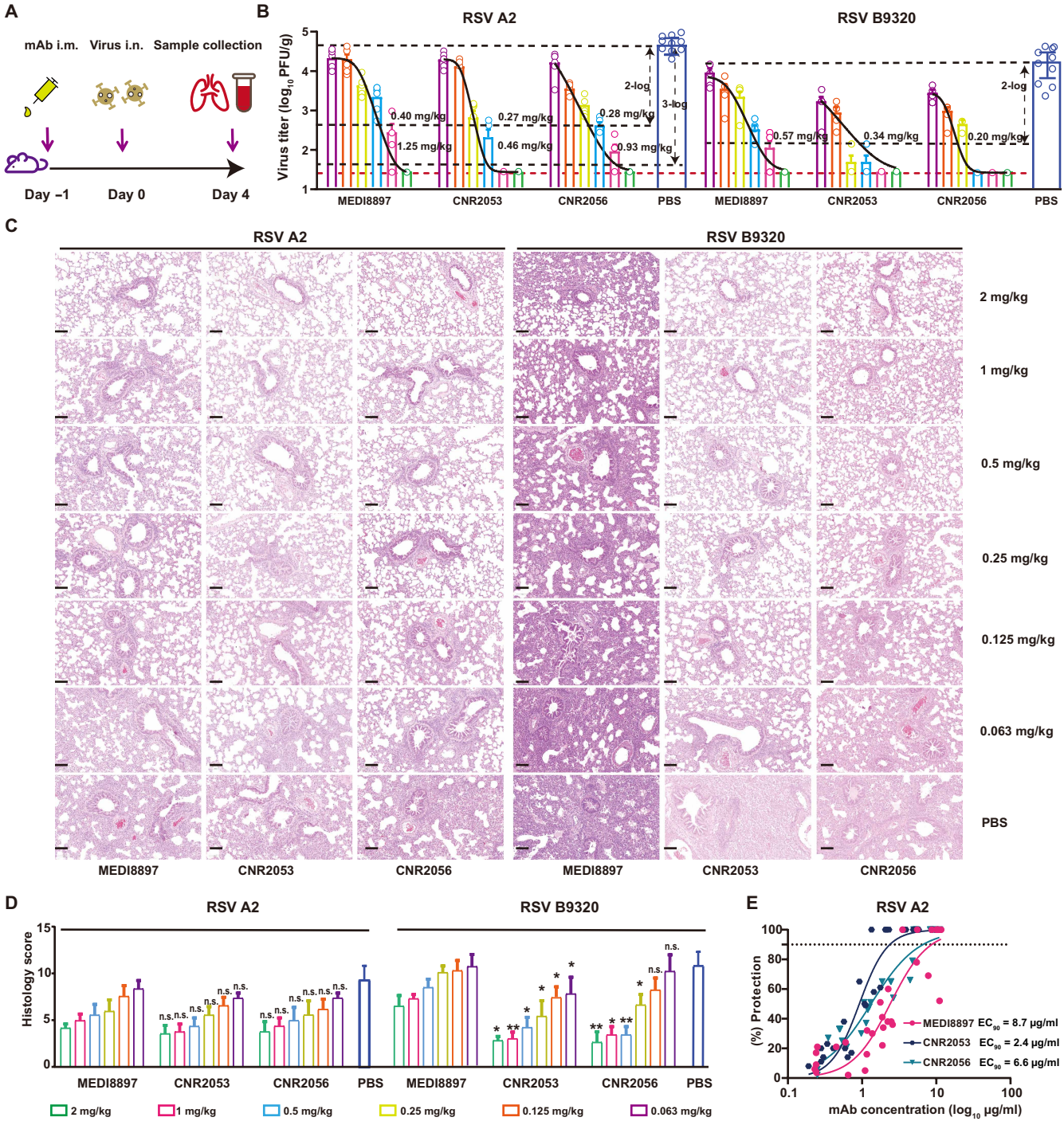

Fig. 2. Prophylactic CNR2053 and CNR2056 confer protection against RSV A2 and B9320 infections in cotton rats. (**A**) Schematic representation of the experimental design for evaluating mAb-mediated protection against RSV infection in the cotton rat model. i.m. = intramuscular; i.n. = intranasal. (**B**) Lung viral titers in cotton rats treated with CNR2053 and CNR2056, measured 4 days after RSV A2 (left) or RSV B9320 (right) challenge, determined by plaque assay. Error bars represent mean values with SD ($n = 5$, except for PBS group with $n = 10$). The black curves represent the nonlinear regression analysis of mAb dose and viral load. The limit of detection for viral load is indicated by the bottom red dashed line. The remaining black dashed lines indicate viral loads that are 100- or 1000-fold lower than those in the PBS group. PFU, plaque-forming units. (**C**) Representative histopathological sections of lungs stained with hematoxylin and eosin (H&E), showing inflammation severity in each group at the indicated mAb doses against RSV A2 (left) or RSV B9320 (right) (magnification, ×200; scale bars, 100 μm). (**D**) Total histology scores of cotton rat lungs infected with RSV A2 (left) or RSV B9320 (right). (**E**) Correlations between serum concentrations of CNR2053 or CNR2056 and inhibition rates of RSV A2 virus titers in the lungs of infected cotton rats were calculated using a nonlinear regression analysis. The dotted line represents EC_{90} for viral reduction. Data are presented as means ± SD. Statistical analysis was performed using the Kruskal-Wallis test followed by Dunn's test for multiple comparisons; data from CNR2053 and CNR2056 were compared with MEDI8897 at the corresponding dose group. $^{*}P < 0.05$ and $^{**}P < 0.01$; n.s., not significant.

passive antibody drugs against RSV, we systematically compared the serum concentrations of CNR2053, CNR2056, and MEDI8897 that correlated with a reduction in RSV titers in the lungs of infected cotton rats and calculated the effective serum concentration yielding a 90% protection (EC_{90}) with a decrease in lung viral titer when compared with control. CNR2053 was calculated to have an EC_{90} value of 2.4 μg/ml against RSV A2. MEDI8897 gave an EC_{90} of 8.7 μg/ml, and CNR2056 exhibited a comparable EC_{90} value to that of MEDI8897 (Fig. 2E). These in vivo results highlight that CNR2053 and CNR2056 exhibit improved prophylactic efficacies compared with currently approved mAb drugs in RSV-infected cotton rats.

The structures of CNR2053 and CNR2056 bound to site Ø reveal the structural basis of unbiased and potent neutralization

To elucidate the epitopes targeted by CNR2056 and CNR2053 and to uncover the molecular basis for their unbiased neutralization against RSV A2 and B9320 strains, we determined the atomic structures of the individual complexes of Fab fragments of CNR2056 and CNR2053 bound to a stabilized RSV pre-F trimer using cryo–electron microscopy (cryo-EM) (fig. S3 and table S3). For each immune complex, three copies of Fabs were bound to one pre-F trimer, with CNR2056, CNR2053, and MEDI8897 Fabs binding to the epitope region at distinct positions and orientations, effectively shielding most of the upper regions (Fig. 3A). CNR2056 binds to a conformational epitope comprising α3 and α4, which is broadly similar to the binding site observed for MEDI8897 (Fig. 3B) (*27*). Specifically, CNR2056 lies behind α4, whereas MEDI8897 binds slightly in front of α4 (Fig. 3B). The interaction surface on CNR2056 involves four complementarity-determining region (CDR) loops, with LCDR1, HCDR2, and HCDR3 extensively surrounding α4 (Fig. 3B and table S4). Tight binding was shown to be facilitated by extensive hydrophilic interactions, including hydrogen bonds and salt bridges, as well as hydrophobic contacts (Fig. 3C and table S4). Unexpectedly, we observed that CNR2053 binds vertically across α4 and α5, leading to the formation of a three-stranded β sheet involving HCDR3 and the linker between α4 and α5, which would normally be extended loops but instead adopt short β strands (Fig. 3B). Structural analysis revealed that the CNR2053 heavy chain dominated the interactions, primarily through LCDR1, HCDR2, and HCDR3 (Fig. 3C). Major interactions involved a network of hydrogen bonds formed by Tyr^{54} (light chain), Asp^{100}, Ser^{105}, Thr^{108}, Ala^{110}, and Thr^{111} in the heavy chain of CNR2053 and Asn^{202}, Lys^{209}, Gln^{210}, Ser^{211}, and Ser^{213} in the pre–F protein and several hydrophobic contacts, including Tyr^{35} (light chain), Val^{102}, Ala^{106}, and Gly^{107}, in the heavy chain of CNR2053 and Pro^{205}, Ile^{206}, Ile^{214}, and Pro^{215} in the pre–F protein (Fig. 3C).

Given that MEDI8897 exhibits compromised potency against some RSV B strains (*28*), such as B18537, whereas CNR2056 and CNR2053 display unbiased activities (Fig. 1), we scrutinized the sequence and conformational alterations in epitope residues recognized by these antibodies. There are three epitope residue substitutions [Asp^{200}→Asn(D200N), Lys^{201}→Asn (K201N), and Lys^{209}→Gln (K209Q)] between the A and B strains, among which the alteration of D200N presumably causes marginal effects because of homologous residues (Fig. 3D). For CNR2056, the alterations of K209Q and K201N abolished one salt bridge with Asp^{31} on LCDR1 but established three new hydrogen bonds with Asp^{31}, Trp^{32} on LCDR1, and Asn^{97} on LCDR3, respectively, in B9320/B18537, further strengthening binding activity (Fig. 3D). This largely matches the in vitro neutralization activity and in vivo protective potency (Figs. 1 and 2). Regarding CNR2053, the alterations of K209Q and K201N only change the interaction type from one salt bridge to one hydrogen bond with Asp^{100} on HCDR3, which may not substantially affect binding capability (Fig. 3D). In contrast, the alterations of K209Q and K201N directly lose one salt bridge with Asp^{92} on LCDR3 and replace two salt bridges with Asp^{101} on HCDR3 and Glu^{55} on LCDR2 by two hydrogen bonds, to some extent reducing the binding affinities of MEDI8897 to B strains (Fig. 3D).

To explore the possibility for broad neutralization and analyze epitope conservation, we constructed an antigenic phylogenetic tree based on all available amino acid sequences of RSV F retrieved from GISAID (Global Initiative on Sharing All Influenza Data), yielding two distinct clades with distinct antigenic drifts, reflected by representative mutations (Fig. 3E). The conservation of epitope residues targeted by the three antibodies was also analyzed using Weblogo from 221 representative strains, revealing several mutation hotspots, including Leu^{172}→Gln (L172Q), D200N, K201N, Ile^{206}→Met (I206M), Lys^{209}→Arg/Gln (K209R/Q), and Ser^{213}→Arg (S213R) (Fig. 3F). These findings indicate a positive correlation between "hot" immunogenic sites and high mutation frequencies. Most mutations in epitope residues have not been reported to markedly reduce potency of MEDI8897, although specific substitutions in clinical isolates, such as Asn^{208}→Ser (N208S), Asn^{208}→Asp (N208D), Asn^{201}→Ser (N201S), and Lys^{68}→Asn (K68N)/Asn^{201}→Ser (N201S), indeed exhibit resistance or even ineffectiveness to MEDI8897 (*17*, *29*–*31*).

HCDR3-driven recognition enables potent cross-reactivity of CNR2047 against RSV and hMPV

CNR2047, which exhibited robust neutralization potency against RSV strains in vitro, also demonstrated high neutralization efficacy against hMPV (Fig. 1F). We evaluated the prophylactic efficacy of CNR2047 in animal models, as detailed in Fig. 2. When administered at doses of ≥1 mg/kg, CNR2047 reduced viral replication of both RSV A2 and B9320 strains by more than 100-fold in cotton rats, showing comparable protective capacities to those of MEDI8897 but slightly weaker efficacies compared with CNR2053 and CNR2056 (Figs. 2B and 4A). In contrast, RSV-199, a previously reported potent cross-neutralization site III mAb, failed to provide prophylactic protection at a dose of 1 mg/kg against either RSV A or B challenge (*18*). The cotton rats treated with CNR2047 at a dose of ≥1 mg/kg exhibited only modest inflammatory cell infiltration and a significant ($P < 0.05$) alleviation of pulmonary histopathological damage (Fig. 4, B and C, and fig. S4). We further tested the in vivo efficacy of CNR2047 against the hMPV A2 strain using a mouse model, given its more efficient infection rate compared with that in cotton rats. Six- to 8-week-old BALB/c mice were administered different doses of CNR2047 1 day before viral challenge with hMPV A2. Doses of 4.5, 1.5, or 0.5 mg/kg of CNR2047 resulted in complete protection from hMPV A2 infection in the lungs and a dose-dependent reduction in pulmonary inflammation, with nearly no detectable pathological injury at the highest dose (Fig. 4, D to F). Thus, CNR2047 not only neutralized both RSV A and B subtypes and hMPV A in vitro but also provided potent protection in animal models.

To elucidate the structural basis for the cross-neutralization of RSV and hMPV by CNR2047, we determined the cryo-EM structures of CNR2047 in complex with RSV or hMPV pre-F to resolutions of

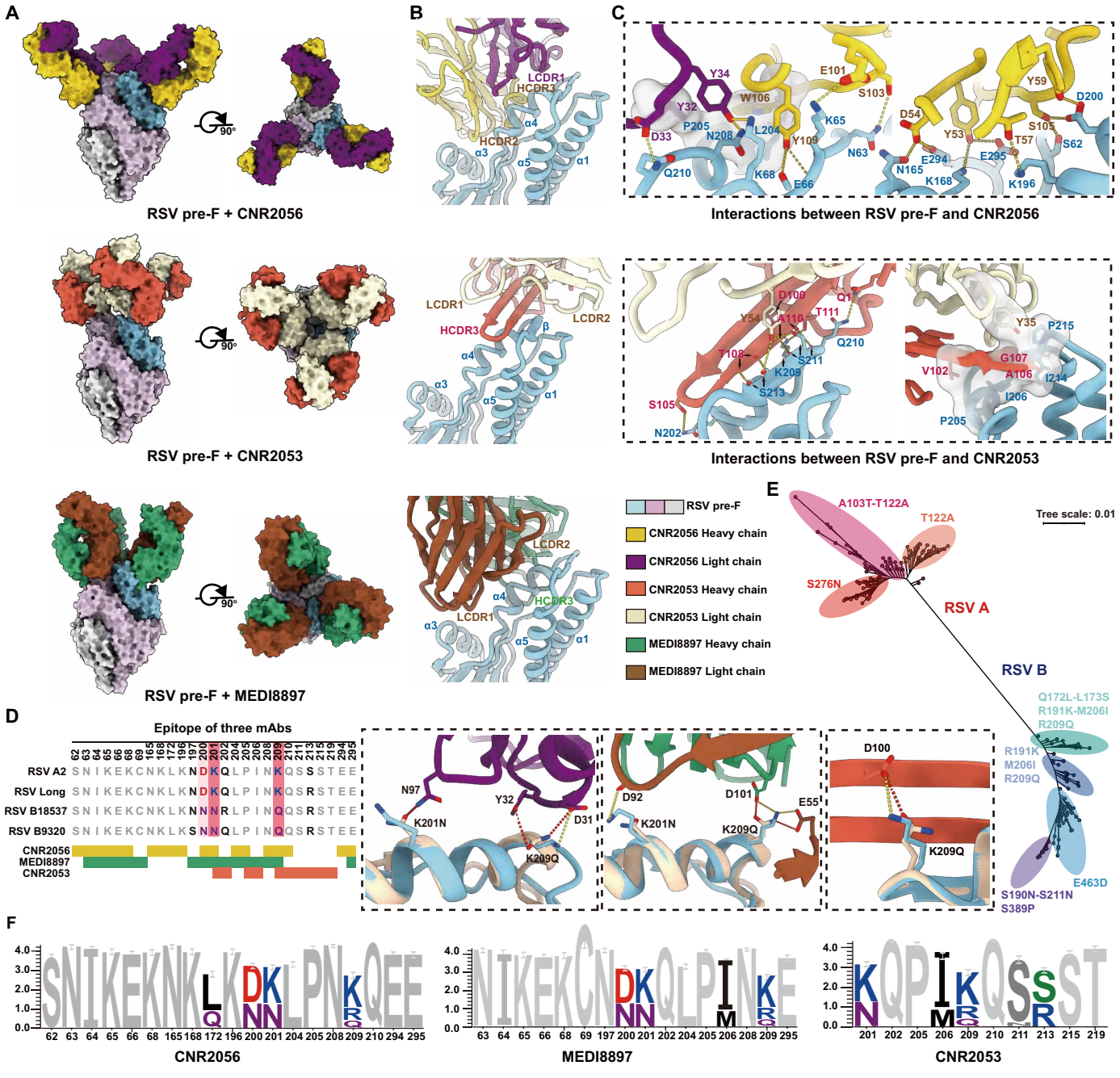

Fig. 3. The structures of CNR2053 and CNR2056 bound to site Ø reveal the structural basis of unbiased and potent neutralization. (**A**) Surface representations of cryo-EM structures of the RSV pre-F trimer (sky blue, thistle, and light gray) in complex with CNR2056 (top, heavy chain: gold; light chain: purple), CNR2053 (middle, heavy chain: tomato; light chain: lemon), and MEDI8897 (bottom, PDB: 5UDC, heavy chain: green; light chain: brown). (**B**) Enlarged views of the binding interfaces to illustrate the binding modes of CNR2056 (top), CNR2053 (middle), and MEDI8897 (bottom). The orientation of RSV pre-F is consistent across panels. The color scheme is consistent with (A). (**C**) Detailed interactions between RSV pre-F and CNR2056 (top) or CNR2053 (bottom). Residues involved in hydrophobic patches and hydrogen bonds are shown as transparent surfaces and labeled, respectively. The color scheme is consistent with (A). (**D**) Structural and epitope analysis of the neutralizing differences of these three antibodies against RSV A2 and RSV B9320. The conserved residues of CNR2053 (tomato), CNR2056 (gold), and MEDI8897 (green) between RSV subtype A and B are shown in gray. Amino acids in the common epitope that differ between RSV subtypes A and B are highlighted for all three antibodies. RSV A2 pre-F and RSV B9320 pre-F are colored in sky blue and peach puff, respectively. The color scheme is consistent with (A). (**E**) Maximum likelihood phylogenetic tree of 221 representative RSV variants built by using MAFFT (v7.505) for multiple sequence alignment and FastTree (v2.1.11) with default parameters. (**F**) Analysis of sequence conservation on residues involved in mAb binding. Logo plots of conservation of epitopes for CNR2056, MEDI8897, and CNR2053 from 221 representative RSV strains are shown. Mutated residues are highlighted in the logo plots.

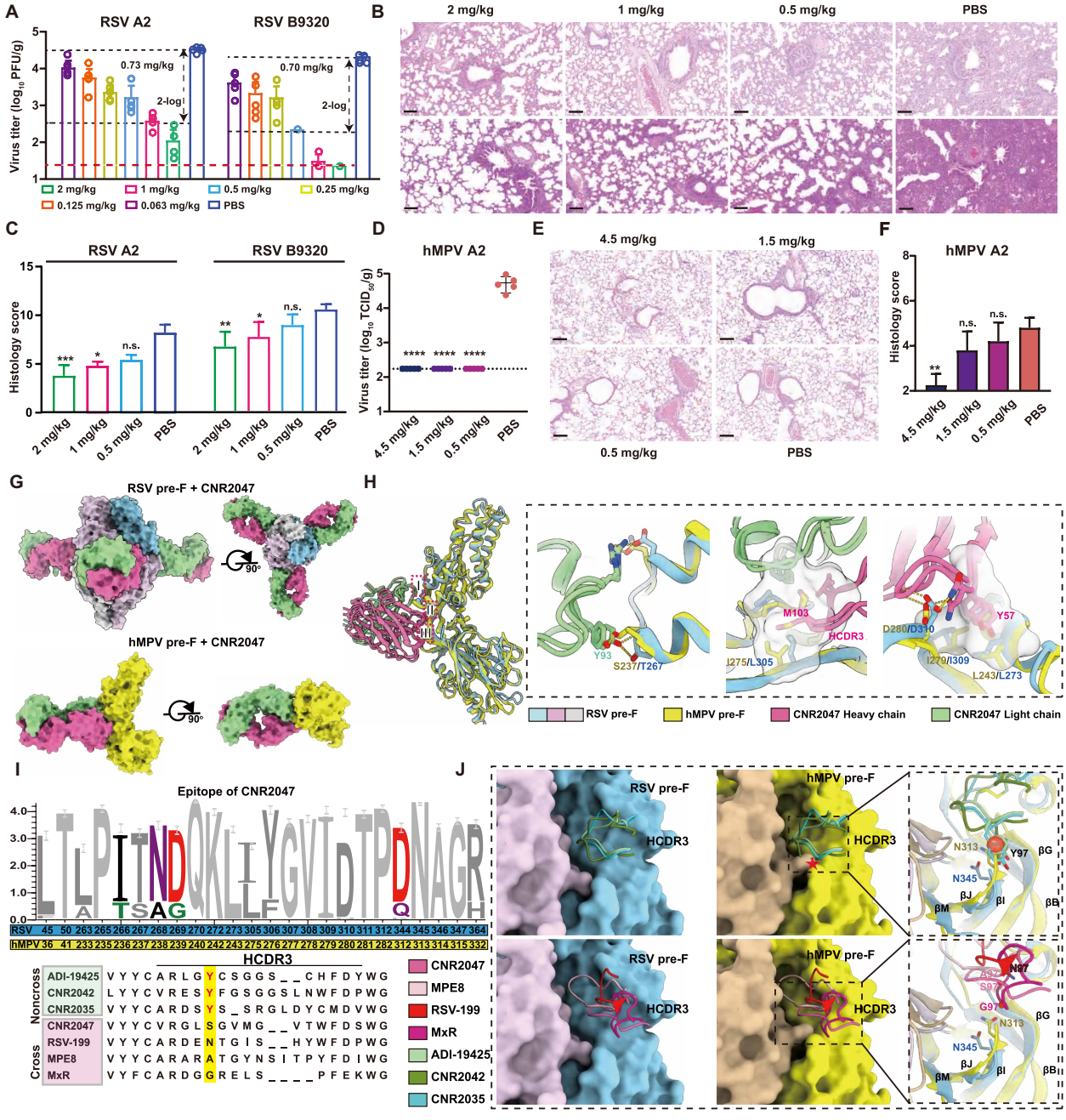

Fig. 4. HCDR3-driven recognition enables potent cross-reactivity of CNR2047 against RSV and hMPV. (**A** to **F**) Cotton rats [(A) to (C)] and BALB/c mice [(D) to (F)] were treated with CNR2047 and challenged with RSV or hMPV, respectively. Animals were infected 1 day later with the indicated strains of RSV or hMPV. Lungs were isolated 4 days later for analysis. [(A) and (D)] Lung viral titers in cotton rats (A) and BALB/c mice (D) treated with CNR2047, measured 4 days after exposure to RSV A2 and RSV B9320 determined by plaque assay or hMPV A2 by Reed-Muench assay. The black dashed lines indicate viral loads that are 100-fold lower than those in the PBS group. The limit of detection for viral load is shown by the bottom red dashed line. Error bars represent mean values with SD ($n = 5$). [(B) and (E)] Representative histopathological sections of cotton rat (B) or BALB/c mouse (E) lungs stained with H&E (magnification, ×200; scale bars, 100 μm). [(C) and (F)] Histology scores are shown for cotton rats (C) and BALB/c mice (F) based on (B) and (E). Data are presented as means ± SD ($n = 5$). Statistical analysis was performed using the Kruskal-Wallis test followed by Dunn's test for multiple comparisons with the PBS group as the control; data from the CNR2047 groups were compared with the PBS group. *$P < 0.05$, **$P < 0.01$, ***$P < 0.001$, and ****$P < 0.0001$; n.s., not significant. $TCID_{50}$, median tissue culture infectious dose. (**G**) Surface representations of cryo-EM structures of CNR2047 (heavy chain: hot pink; light chain: pale green) in complex with the RSV pre-F trimer (top, sky blue, thistle, and light gray) or hMPV pre-F monomer (bottom, yellow). (**H**) Structure-based analysis of CNR2047's cross-neutralizing activity. Details of the interactions are shown on the right and framed by dashed lines. Residues involved in hydrophobic patches and hydrogen bonds are shown as transparent surfaces and labeled, respectively. The color scheme is consistent with (G). (**I**) Logo plot of sequence conservation analysis of the epitope for CNR2047 from 221 representative RSV strains and 55 hMPV variants. Residues are colored on the basis of their conservation and chemical properties. The HCDR3 differences in sequence lengths of mAbs are shown in the table below the logo plot. Cross indicates cross-reactivity with RSV and hMPV; noncross indicates RSV specific. (**J**) Structure-based analysis of RSV-specific mAbs (CNR2035, CNR2042, and ADI-19425) for their lack of cross-reactivity with hMPV.

3.8 and 4.1 Å, respectively (Fig. 4G and fig. S5). Unlike the trimeric structure of RSV F, each CNR2047 Fab fragment formed a 1:1 complex with individual hMPV monomers (Fig. 4G), similar to the structural observations for RSV-199 (*18*). CNR2047 primarily targeted a conserved epitope (site III) across RSV and hMPV strains with a root mean square deviation (RMSD) of 1.031 Å, analogous to the binding modes of RSV-199, MPE8, MxR, and ADI19425 (*18*, *32*–*34*) (fig. S6). Comparisons of the footprints of the CNR2047 CDRs on RSV and hMPV F revealed nearly identical contacts with the two pre–F proteins, despite local sequence differences, mediated by hydrophilic and hydrophobic interactions from three major patches (Fig. 4H). Weblogo analysis of 277 representative strains showed that 83.3% of residues comprising the CNR2047 epitope were conserved across all four RSV and hMPV subtypes (Fig. 4I and fig. S7). In contrast, more than 65% of epitope residues targeted by site Ø antibodies were highly diverse, with most mutations involving major alterations in surface charge, distinguishing the antigenicity between RSV and hMPV (fig. S7).

To further understand the subtle and specific variations between RSV and hMPV in the engagement by site III–directed antibodies derived from the same germline heavy (*IGHV3-21*) and light chain (*IGLV1-40*), we compared the structural differences between two subgroups: cross-reactive antibodies (e.g., CNR2047, RSV-199, MPE8, and MxR) (*18*, *32*, *33*) and RSV-specific mAbs (e.g., ADI19425, CNR2035, and CNR2042) (*34*) (fig. S8 and table S5). Although the sequences and structures of CDR1s and CDR2s were highly conserved across all mAbs, with limited variations in LCDR3, the HCDR3s showed marked differences in sequence lengths and configurations (Fig. 4I and fig. S8), indicating a critical role for HCDR3 in cross-reactivity. All HCDR3s recognized a cavity formed by two adjacent F monomers, with MPE8 HCDR3 being the longest and most buried (Fig. 4J). The HCDR3s of all three RSV-specific mAbs contained the residue Tyr^{97}, which appeared to cause steric clashes with Asn^{313} in hMPV, but not in RSV, due to a minor conformational shift in the βI-βJ loop (Fig. 4J). In contrast, all cross-reactive antibodies had a small side-chain residue at position 97 in HCDR3, allowing flexible fitting into the cavity and enabling cross-reactivity (Fig. 4J).

DMS and clinical isolates identify escape hotspots but confirm retained potency of CNR2056 and CNR2047 against RSV variants

Although the frequency of mutations in epitope residues can provide insights into potential escape risks for antibodies, relying on only structural data reveals the contacting residues and does not identify genuine escape mutations for specific mAbs. Recent advances in deep antigen mutation screening (DMS) using a fluorescence-activated cell sorting (FACS)–based cell display platform have enabled the mapping of all single amino acid mutations in the target antigen that affect the binding of mAbs (*35*, *36*). To evaluate immunological tolerance and map key escape mutation sites, we characterized the profile of RSV F escape mutations for representative mAbs binding sites Ø and III using DMS assays (*37*–*39*) (Fig. 5A), where higher escape scores indicated stronger disruption of antibody binding by the corresponding mutations. The escape mutation profiles indicated that MEDI8897 is sensitive to specific substitutions at positions Leu^{204}, Lys^{209}, Pro^{205}, Lys^{196}, Asn^{208}, Lys^{201}, and Asp^{200}. This sensitivity was corroborated by previously reported resistant strains with mutations such as K209Q/D200N/K201N/Gln^{202}→Arg(Q202R) observed in B18537 and N208S, N208D, N201S, and K68N/N201S identified in clinically escaped strains (*17*, *29*–*31*) (Fig. 5, A and B). Similarly, changes at positions Leu^{204}, Ile^{64}, Lys^{196}, Pro^{205}, and Lys^{168} impaired the binding activity of CNR2056, whereas substitutions at positions Ser^{211}, Ile^{206}, Glu^{294}, and Pro^{205} compromised CNR2053 (Fig. 5, A and B). Three continuous residues located around the terminus of the α4 helix, namely, Leu^{204}, Pro^{205}, and Ile^{206}, form a hydrophobic patch that can engage with hydrophobic paratope residues of all three mAbs. Structurally, these presumably ensure the correct conformation for the α4-α5 region by terminating α4 with Pro^{205}, thereby conferring high escape scores (Figs. 3 and 5, A and B). These might indicate a high escape barrier to overcome the Pro^{205} mutation. Residue substitutions at positions Thr^{50}, Thr^{267}, Gln^{270}, Asp^{310}, and Gly^{307}, which are highly conserved across RSV and hMPV, conferred resistance to CNR2047 (Fig. 5, A and B). To address concerns about potential immune evasion from real-world variants, we constructed a mutational heatmap using RSV F sequences obtained from publicly accessible databases [National Center for Biotechnology Information (NCBI), European Bioinformatics Institute (EBI), and GISAID] and analyzed the mutational diversity and accumulation over time at key escape sites (Fig. 5, C to E). Five residues at positions 200, 201, 206, 209, and 211, with high mutational frequencies and diversities, were identified as potential immune evasion sites. Among these, substitutions of K209R, I206M, and Ser^{211}→Asn (S211N) have gradually outcompeted other mutations in RSV variants and are widely observed in recent prevailing variants (Fig. 5E). These findings suggest that MEDI8897 and CNR2053 are at relatively high risk of specific clinical RSV strains exhibiting resistance. To further verify these findings, we evaluated a panel of 24 recently isolated RSV clinical variants (16 RSV-A and 8 RSV-B) with representative mutations for potential immune evasion (fig. S9). Four RSV-B strains displayed moderate resistance (10- to 30-fold) to MEDI8897 because they harbored mutations like Lys^{201}→Ser (K201S), K201N, Q202R, and K209Q. One isolate with I206M/S211N substitutions decreased the neutralizing potency of CNR2053 by 170-fold (Fig. 5F). However, CNR2056 and CNR2047 could broadly neutralize all tested RSV-A and RSV-B isolates; the same breadth was found for the cross-neutralizing antibody MPE8. We did not identify RSV clinical isolates with key escape mutations for CNR2056 and CNR2047 in the public sequence datasets we analyzed. Alterations such as S211N and I206M resulted in the loss of one hydrogen bond with Tyr^{54} on LCDR2 and slight clashes with Thr^{104} on HCDR3, respectively, thereby reducing the binding affinity and neutralizing potency for CNR2053 (fig. S10). Similarly, the mutation Asn^{208}→Tyr (N208Y) caused severe clashes with Tyr^{100} on HCDR3, and changes of either N201S or N208S appeared to decrease hydrophilic contacts, possibly driving compromised binding by MEDI8897 (fig. S10). In summary, both CNR2056 and CNR2047 exhibited broad and potent binding activities against tested variants with minimal immune evasion potential.

Cocktail therapies confer cross-protection and mitigate mutational escape

Each of the three antibodies, CNR2053, CNR2056, and CNR2047, demonstrated potent neutralizing activity and provided effective protection in animal models. These findings enabled us to rationally design two mAb cocktails combining site Ø–targeting antibodies (CNR2053 or CNR2056) with the site III–targeting mAb CNR2047. We initially assessed the simultaneous binding of CNR2047 and the

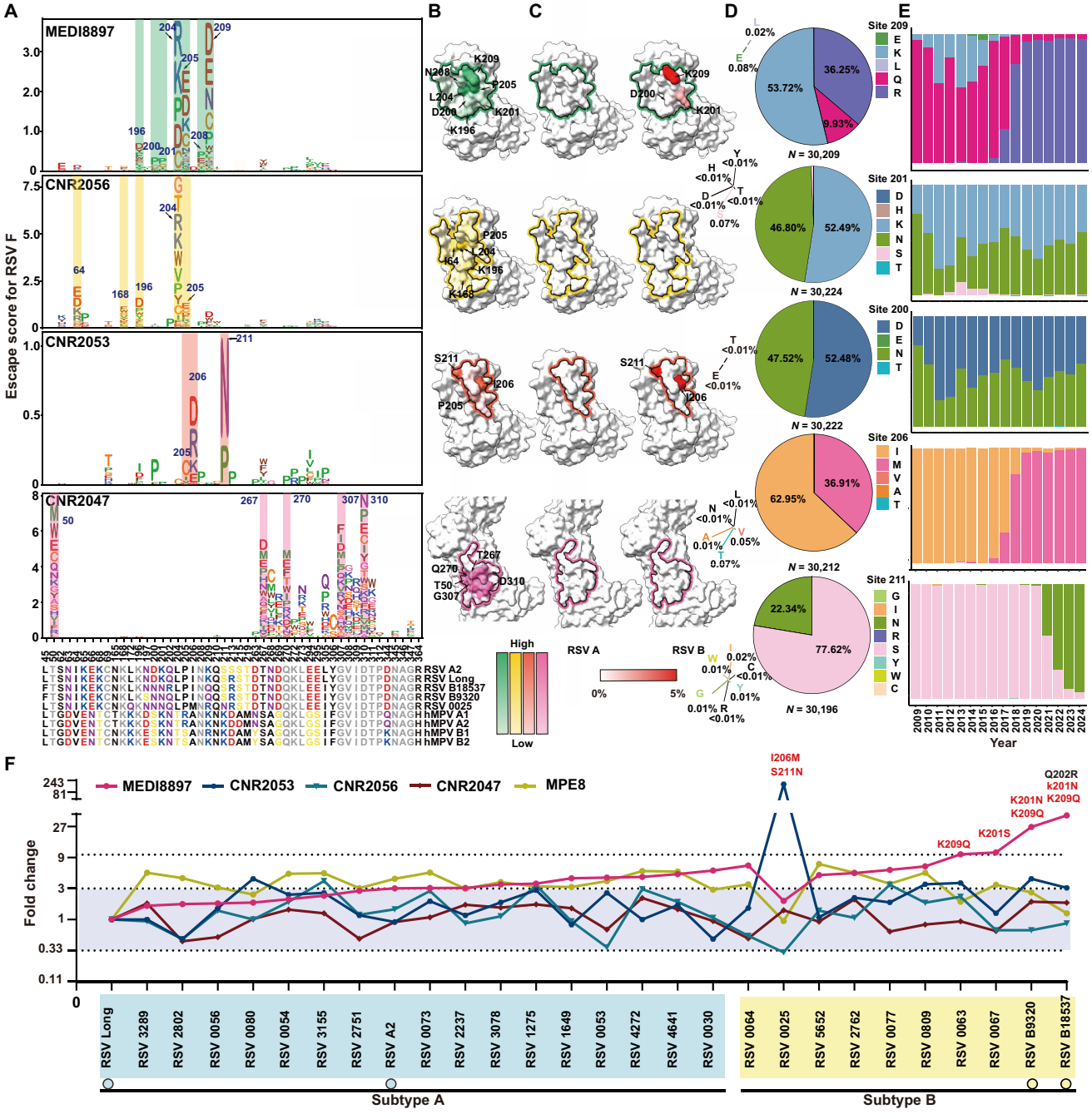

Fig. 5. DMS and clinical isolates confirm retained potency of CNR2056 and CNR2047 against RSV variants. (**A**) Escape mutational profiles for RSV F binding activity derived from DMS results (top) and epitope amino acid conservation analysis of sites Ø and III (bottom). Escape scores for mAbs are shown in the top graphs, with top escape residues highlighted in green (for MEDI8897), yellow (CNR2056), orange (CNR2053), and magenta (CNR2047). Higher escape scores indicate stronger disruption of antibody binding by the corresponding mutations. The logo plot letter height in the top graph corresponds to the escape score for RSV F in binding activity. The bottom sequence alignment shows the epitope amino acid conservation of sites Ø and III between diverse RSV strains and hMPV strains. When the residue is conserved, amino acids are shown in gray; when variable, hydrophobic residues (A, L, I, P, F, and M) are black, polar residues (G, S, and T) are yellow, neutral residues (Q and N) are purple, and acidic residues (D and E) are red. (**B**) Surface representations of epitope escape risk in mAbs for RSV F, colored as in (A), with arrows indicating critical escape residues. (**C**) Shown is the conservation of mAb high-escape residues identified by DMS for RSV F in (A) across publicly available sequences of RSV-A (left) and RSV-B (right) subtypes. As shown in the color bar, conservation ranges from 0 to 5%; greater sequence variation is indicated by increasingly red shading. (**D** and **E**) Prevalences of key amino acid mutations in the RSV F protein are presented in total as a pie chart (D) and over time as a bar chart (E) from publicly accessible databases (NCBI, EBI, and GISAID), with diverse mutations represented by different colors; diverse mutations counting less than 0.1% are shown on the left side of the pie charts. (**F**) Fold change in mAb neutralization against RSV clinical isolates compared with the RSV long strain. Fold changes in IC_{50} of less than 3 are shaded in light purple, and the top dashed line indicates a fold change of 10. Key mutation residues of RSV strains identified as functionally critical by DMS are labeled in red when the fold change is greater than 10; the remaining residues are shown in black. The circles at the bottom indicate RSV laboratory strains.

two site Ø–targeting antibodies to RSV pre-F using competitive BLI (Fig. 6A). The nitrilotriacetic acid (NTA) sensor, labeled with RSV pre-F, was saturated with CNR2047 and subsequently exposed to CNR2053 or CNR2056 in the flow-through, or vice versa. As expected, CNR2047's binding did not interfere with the attachment of CNR2053 or CNR2056 to RSV pre-F, highlighting the potential for these antibodies to form cooperative dual-mAb cocktails (Fig. 6A). Although CNR2053 and CNR2056 did not inhibit hMPV individually, the mAb cocktails CNR2053-CNR2047 and CNR2056-CNR2047 exhibited expanded breadth and neutralizing activity against all RSV variants tested and against hMPV, thereby potentially reducing mutational escape risks raised from RSV (Fig. 6, B and C). We further evaluated the preclinical efficacy of these mAb cocktails as prophylaxes against RSV and hMPV infections in animal models. As anticipated, cocktails of CNR2053-CNR2047 or CNR2056-CNR2047 administered at a dose of 0.5 mg/kg reduced viral replication of RSV A2, B9320, and hMPV A2 strains by more than 100-fold compared with PBS. Higher doses of 2 mg/kg achieved complete protection in the lungs against RSV A2, B9320, and hMPV A2 challenges (Fig. 6, D and E). A low dose of 1 mg/kg of CNR2053-CNR2047 resulted in complete clearance of RSV A2 and B9320 from the lungs, whereas a dose of 0.5 mg/kg of CNR2056-CNR2047 provided complete protection against hMPV A2 infection (Fig. 6, D and E). Furthermore, animals receiving doses of ≥0.5 mg/kg exhibited only mild peribronchiolitis and interstitial inflammation (Fig. 6, F and G, and fig. S11). To elucidate the molecular basis for the cross-protective effect of these dual-mAb cocktails, we performed cryo-EM analysis of the RSV pre-F trimer in complex with CNR2053-CNR2047 or CNR2056-CNR2047 (fig. S12). Unlike most structures of apo RSV pre-F or its complexes with antibodies, which typically exhibit homogeneous trimeric architectures (*11*, *40*, *41*), we observed a heterotrimeric complex composed of one RSV F protomer, CNR2056, and CNR2047, existing in monomeric (52%), dimeric (38%), and trimeric (10%) assembly states, with RMSD values of less than 1 Å relative to the best-fit atomic model (Fig. 6H). This suggests that the binding of CNR2056 and CNR2047 possibly facilitates the disassembly of the stable pre-F trimer, which might provide the mechanistic basis for RSV and hMPV neutralization in addition to other unknown mechanisms (Fig. 6H). In contrast, we found that the pre-F–CNR2053–CNR2047 complex exists in a single trimeric state with six Fab fragments bound to one pre-F trimer. We observed that three CNR2053 Fabs bound on the top of the pre-F trimer, forming a cap layer (shield-1), and that three CNR2047 Fabs bound on the side, creating an exterior layer (shield-2) with a staggered array beneath the cap layer (Fig. 6, H and I). These two layers may act as a shield to mask most of the upper regions of the F trimer, presumably blocking viral attachment to the host cell. In addition, all three mAbs specifically recognize the pre-F conformation rather than the post–F protein, indicating conformational changes in the epitope regions during the viral fusion process. These suggest that the six Fab fragments may work to restrain further conformational changes from the pre-F to the post-F state, which is essential for initiating viral fusion. These structural insights may explain the molecular basis for the neutralization mechanism of RSV by the mAb cocktails and provide a rationale for formulating two types of neutralizing antibodies. The cooperativity of two noncompeting antibodies—one targeting a more conserved epitope across RSV and hMPV and the other targeting an RSV-specific patch—confers potent and broad protection against these human pneumoviruses.

DISCUSSION

Passive immunization through RSV F–specific neutralizing antibodies stands as a well-established and desirable strategy to protect infants against RSV infection with a superior safety profile. We reasoned that health care workers, particularly pediatricians with long-term occupational exposure to respiratory viruses such as RSV and hMPV, serve as an underexplored repertoire to isolate highly potent neutralizing antibodies. From 57 RSV F protein–specific memory B cells isolated from pediatricians, we obtained three highly potent (CNR2056, CNR2053, and CNR2047) mAbs harboring high SHM rates (>10% in V_H), a higher efficiency compared with conventional discovery approaches (*15*). CNR2053 and CNR2056 demonstrated 1.5- to 25-fold and 5- to 20-fold higher neutralization potency compared with the clinical benchmark MEDI8897 and MK-1654, respectively, and showed unbiased neutralizing activity against RSV A and B strains. Moreover, 67% of the isolated mAbs specifically targeted the immunodominant Ø or III sites of the pre–F protein, with the majority exhibiting neutralizing activity. The enhanced mAb potency presumably correlates with long-term repeated viral exposure (median duration of more than 10 years of work in pediatrics in our cohort), which may continuously drive affinity maturation. This is supported by the high SHM rates observed in the isolated mAbs, consistent with the established paradigm that chronic or repeated antigen stimulation can promote B cell receptor optimization, leading to antibodies with exceptional neutralization breadth and potency (*42*). These findings collectively highlight both the efficiency and quality of mAb discovery from repeatedly exposed health care workers.

Our structural and functional analyses have unveiled critical insights into the differential escape profiles of site Ø–directed antibodies. These mAbs are high-quality, RSV-specific antibodies with robust activity. However, despite the subtle differences in the epitopes of these antibodies, we observed substantial variation in the key sites that determine binding activity and potential to escape immune pressure. Although antibodies targeting site Ø are relatively abundant, the high immune pressure on this site may drive viral escape. The hydrophobic patch comprising L204 and P205, located at the terminus of the α4 helix, represents an evolutionarily constrained region where mutations are strongly disfavored because of their destabilizing effects on the pre-F conformation. This explains the resilience of CNR2056, which targets this region. Particularly notable is CNR2053's distinct mechanism: Its HCDR3 forms a three-stranded β sheet with the α4-α5 linker, forcibly restructuring a normally flexible loop region. This unconventional binding mode underlies its picomolar potency but creates a vulnerability: Substitutions at Ser^{211} (e.g., S211N) would disrupt critical hydrogen bonds with HCDR3, whereas an I206M mutation introduces steric clashes. A combination of these mutations can therefore enable viral escape. The high prevalence of such escape variants in clinical isolates suggests that CNR2053-like antibodies may be common in human RSV–specific immune responses, driving selection pressure. These findings highlight how atomic-level understanding of antibody-paratope interactions can predict both neutralization potency and evolutionary escape pathways.

The identification of HCDR3 as a primary determinant of cross-reactivity among site III–targeting antibodies against RSV and hMPV holds implications for understanding the molecular basis of mAb specificity and for the development of broad-spectrum antiviral agents. Our findings underscore the critical role of HCDR3 sequence

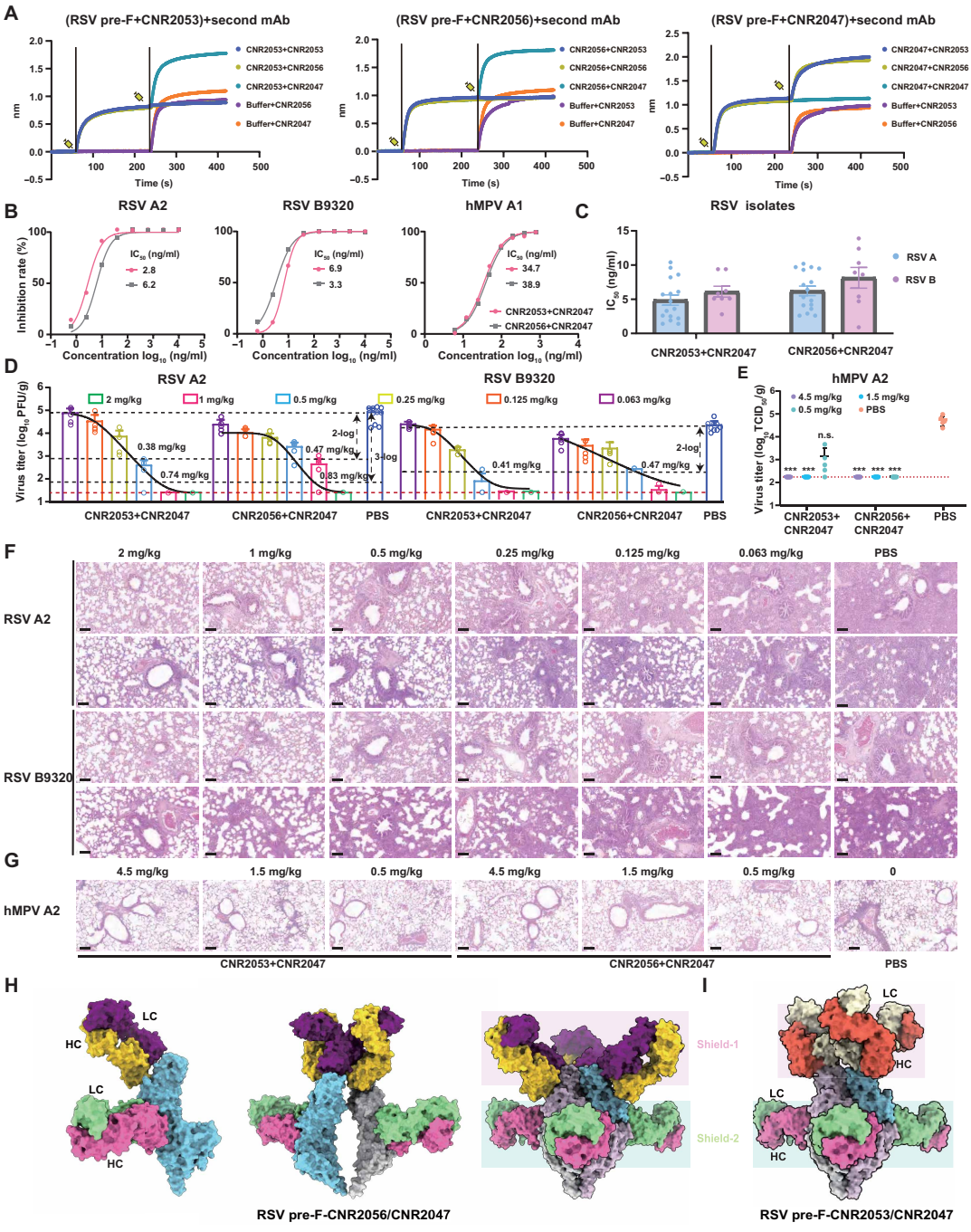

Fig. 6. mAb cocktails exhibit broad activity against RSV and hMPV. (**A**) Competitive binding of CNR2053, CNR2056, and CNR2047 to RSV pre-F detected by BLI. RSV pre-F was immobilized onto the sensor. CNR2053 was first injected, followed by CNR2053, CNR2056, or CNR2047. Similarly, CNR2056 or CNR2047 was first injected, followed by the three mAbs. (**B** and **C**) Neutralizing activity of mAb cocktails CNR2053/CNR2047 and CNR2056/CNR2047 against RSV A2, RSV B9320, and hMPV A1 (B) as well as clinical RSV isolates (C) determined by the PRNT. Error bars represent mean values with SEM ($n = 16$ for RSV A isolates; $n = 8$ for RSV B isolates). (**D** and **E**) Cotton rats (D) and BALB/c mice (E) were prophylactically administered (i.m.) mAb cocktails or PBS control and then infected the next day with the indicated strains of RSV and hMPV (i.n.); viral loads in the lungs were measured 4 days after exposure to RSV A2, RSV B9320, and hMPV A2 by plaque assay (RSV) and Reed-Muench assay (hMPV). Error bars represent mean values with SD [$n = 5$, except for PBS group with $n = 10$ in (D)]. The black curves represent the nonlinear regression analysis of mAb dose and viral load. The limit of detection for viral load is indicated by the bottom red dashed line. The remaining black dashed lines indicate viral loads that are 100- or 1000-fold lower than those in the PBS group. (**F** and **G**) Representative histopathological sections of lung tissues stained with H&E (magnification, ×200; scale bars, 100 μm) from cotton rats and BALB/c mice, showing the extent of inflammatory cell infiltration in each group at the indicated mAb cocktail doses against RSV A2 (top) and RSV B9320 (bottom) (F) and hMPV A2 (G). Statistical analysis was performed using the Kruskal-Wallis test followed by Dunn's test for multiple comparisons with the PBS group as the control; data from the mAb cocktail group were compared with the PBS group. ***$P < 0.001$; n.s., not significant. (**H** and **I**) Surface representations of cryo-EM structures of RSV pre-F in complex with CNR2047/CNR2056 (H) and CNR2047/CNR2053 (I). Three binding patterns were identified for the CNR2047/CNR2056-RSV pre-F complex: monomeric binding (left), dimeric interface engagement (middle), and trimeric symmetry-adapted binding (right). CNR2053/CNR2056 Fabs bind at the top of RSV pre-F, forming the shield-1; CNR2047 Fabs bind at the side, constructing an exterior layer (shield-2). HC, heavy chain; LC, light chain. RSV pre-F trimer (sky blue, thistle, and light gray); CNR2056 (HC, gold; LC, purple), CNR2053 (HC, tomato; LC, lemon); CNR2047 (HC, hot pink; LC, pale green).

and structural features in dictating mAb cross-reactivity (e.g., CNR2047, RSV-199, and MPE8), highlighting the importance of this region in mediating interactions with viral antigens. Specifically, the absence of bulky residues (e.g., Tyr^{97} in RSV-specific counterparts) enables the HCDR3 to engage a conserved cavity formed by adjacent F protomers without steric clashes with hMPV-specific residues like Asn^{313}. However, cross-reactivity appeared to be further modulated by ancillary factors: (i) CDR1/CDR2 fine-tuning through

SHM, as seen in CNR2047's enhanced affinity over RSV-199 because of optimized charge complementarity, and (ii) framework mutations that stabilize the paratope conformation, explaining CNR2047's superiority to RSV-199/MPE8/MxR despite shared germline origins.

The conservation of site III (83.3% residue identity across RSV/hMPV genotypes) positions it as an ideal target for broad-spectrum protection. By combining CNR2047 (site III) with site Ø–directed antibodies (e.g., CNR2056/CNR2053), we achieved multiple benefits: (i) expanded neutralization breadth to encompass more pneumovirus genotypes and (ii) a potentially higher escape barrier for RSV, given that simultaneous mutations in both epitopes may impose prohibitive fitness costs. This dual-target strategy mirrors successful sarbecovirus mAb cocktails (*43*), offering a blueprint for overcoming viral diversity in respiratory pathogens.

Although our study provides comprehensive structural and functional insights into a panel of potent RSV- and hMPV-neutralizing antibodies, several limitations must be acknowledged. First, DMS was restricted to RSV F. Generating hMPV F DMS datasets is an immediate priority of our ongoing work. Second, the neutralizing activity for the cross-reactive mAb CNR2047 is limited to hMPV subtype A. Although binding assays suggest activity against hMPV-B F, we lack neutralization and challenge data for subtype B because of the unsuccessful isolation of subtype B strains. Third, the hypothesis that the mAb cocktail raises the RSV escape barrier remains to be validated with a larger panel of contemporary circulating strains. Last, the current cohorts of repeatedly RSV- and hMPV-exposed health care workers and healthy volunteers remain limited in size. Expanding these groups is essential to more accurately quantify the impact of recurrent exposure on antibody evolution and potency.

In conclusion, by leveraging natural immunity in repeatedly exposed individuals, we identified mAbs with high potency against RSV and hMPV. Their structural and functional characterization not only advance our mechanistic understanding but also pave the way for broad-spectrum immunoprophylaxis against pneumoviruses. This CNR2056-CNR2047 cocktail, deliverable in a single low-dose injection, may offer a versatile, broad-spectrum immunoprophylactic that shields the most vulnerable from present and future pneumoviruses.

MATERIALS AND METHODS

Study design

This study was designed to develop broad-spectrum cross-neutralizing mAb candidates for passive immunization against RSV and hMPV in pediatric populations. A panel of RSV mAbs was generated from human B cells donated by pediatricians with occupational RSV exposure and screened for in vitro functional activity, including ELISA, RSV and hMPV neutralizing assays with technical replicates, and BLI. Sample collection was approved by the Institutional Review Board of Children's Hospital of Chongqing Medical University (2021-343-1). mAbs with the highest activity or cross-neutralizing activity against RSV and hMPV were selected for further exploration of their protective efficacy in diverse RSV subtype–infected cotton rats and hMPV-infected mice. Cryo-EM structures of their Fabs bound to RSV/hMPV pre-F defined epitopes and neutralization mechanisms. Deep mutational scanning and clinical isolate testing assessed escape risk. Epitope uniqueness and conservation guided formulation of mAb cocktails whose RSV/hMPV neutralizing activities were verified in vitro and in vivo. All animal research was approved by the Institutional Biomedical Research Ethics Committee of the Institute of Biophysics, Chinese Academy of Sciences. All animal procedures were conducted in strict accordance with established animal guidelines. Animals were randomly assigned to different groups with $n = 5$ or 10. The sample sizes were derived from preliminary experiments or previous studies. All samples were included in all of the experiments. All histology scores and virus titer assessments were performed by an investigator blinded to the experimental conditions.

Statistical analysis

Individual-level data are presented in data file S1. Statistical analysis was performed using GraphPad Prism10.1.2 by the Kruskal-Wallis test followed by Dunn's test for multiple comparisons except for data in figs. S1A and S4C, which were analyzed by the Mann-Whitney *U* test. An alpha value of 0.05 was considered significant. $*P < 0.05$, $**P < 0.01$, $***P < 0.001$, and $****P < 0.0001$; n.s., not significant.

Supplementary Materials

The PDF file includes:
Materials and Methods
Figs. S1 to S12
Tables S1 to S6
References (*45*–*55*)

Other Supplementary Material for this manuscript includes the following:
Data file S1
MDAR Reproducibility Checklist

REFERENCES AND NOTES

1. K. M. Edwards, Y. Zhu, M. R. Griffin, G. A. Weinberg, C. B. Hall, P. G. Szilagyi, M. A. Staat, M. Iwane, M. M. Prill, J. V. Williams, New Vaccine Surveillance Network, Burden of human metapneumovirus infection in young children. *N. Engl. J. Med.* **368**, 633–643 (2013).
2. N. M. Scheltema, A. Gentile, F. Lucion, D. J. Nokes, P. K. Munywoki, S. A. Madhi, M. J. Groome, C. Cohen, J. Moyes, K. Thorburn, S. Thamthitiwat, H. Oshitani, S. P. Lupisan, A. Gordon, J. F. Sánchez, K. L. O'Brien, PERCH Study Group, B. D. Gessner, A. Sutanto, A. Mejias, O. Ramilo, N. Khuri-Bulos, N. Halasa, F. de-Paris, M. R. Pires, M. C. Spaeder, B. A. Paes, E. A. F. Simões, T. F. Leung, M. T. da Costa Oliveira, C. C. de Freitas Lázaro Emediato, Q. Bassat, W. Butt, H. Chi, U. B. Aamir, A. Ali, M. G. Lucero, R. A. Fasce, O. Lopez, B. A. Rath, F. P. Polack, J. Papenburg, S. Roglić, H. Ito, E. A. Goka, D. E. Grobbee, H. Nair, L. J. Bont, Global respiratory syncytial virus-associated mortality in young children (RSV GOLD): A retrospective case series. *Lancet Glob. Health* **5**, e984–e991 (2017).
3. J. S. Nguyen-Van-Tam, M. O'Leary, E. T. Martin, E. Heijnen, B. Callendret, R. Fleischhackl, C. Comeaux, T. M. P. Tran, K. Weber, Burden of respiratory syncytial virus infection in older and high-risk adults: A systematic review and meta-analysis of the evidence from developed countries. *Eur. Respir. Rev.* **31**, 220105 (2022).
4. X. Wang, Y. Li, T. Shi, L. J. Bont, H. Y. Chu, H. J. Zar, B. Wahi-Singh, Y. Ma, B. Cong, E. Sharland, R. D. Riley, J. Deng, J. Figueras-Aloy, T. Heikkinen, M. H. Jones, J. G. Liese, J. Markić, A. Mejias, M. C. Nunes, B. Resch, A. Satav, K. T. Yeo, E. A. F. Simões, H. Nair, Respiratory Virus Global Epidemiology Network, RESCEU investigators, Global disease burden of and risk factors for acute lower respiratory infections caused by respiratory syncytial virus in preterm infants and young children in 2019: A systematic review and meta-analysis of aggregated and individual participant data. *Lancet* **403**, 1241–1253 (2024).
5. K. Mohammadi, S. Faramarzi, S. Yaribash, Z. Valizadeh, E. Rajabi, M. Ghavam, R. Samiee, B. Karim, M. Salehi, A. Seifi, M. Shafaati, Human metapneumovirus (hMPV) in 2025: Emerging trends and insights from community and hospital-based respiratory panel analyses—A comprehensive review. *Virol. J.* **22**, 150 (2025).
6. S. Esposito, M. V. Mastrolia, Metapneumovirus infections and respiratory complications. *Semin. Respir. Crit. Care Med.* **37**, 512–521 (2016).
7. J. Papenburg, M.-È. Hamelin, N. Ouhoummane, J. Carbonneau, M. Ouakki, F. Raymond, L. Robitaille, J. Corbeil, G. Caouette, L. Frenette, G. De Serres, G. Boivin, Comparison of risk factors for human metapneumovirus and respiratory syncytial virus disease severity in young children. *J. Infect. Dis.* **206**, 178–189 (2012).
8. M. Melgar, A. Britton, L. E. Roper, H. K. Talbot, S. S. Long, C. N. Kotton, F. P. Havers, Use of respiratory syncytial virus vaccines in older adults: Recommendations of the advisory

committee on immunization practices—United States, 2023. *MMWR Morb. Mortal. Wkly. Rep.* **72**, 793–801 (2023).
9. M. D. Snape, J. Moore, J. Du, C. Reuter, N. Penn, S. K. Stoszek, C. A. Shaw, Safety and immunogenicity of an mRNA-based RSV vaccine and an RSV/hMPV combination vaccine in children 5 to 23 months of age. Preprints 202412087 [Preprint] (2024). https://doi.org/10.20944/preprints202412.0878.v1.
10. M. S. A. Gilman, P. Furmanova-Hollenstein, G. Pascual, A. B. van 't Wout, J. P. M. Langedijk, J. S. McLellan, Transient opening of trimeric prefusion RSV F proteins. *Nat. Commun.* **10**, 2105 (2019).
11. A. Krarup, D. Truan, P. Furmanova-Hollenstein, L. Bogaert, P. Bouchier, I. J. M. Bisschop, M. N. Widjojoatmodjo, R. Zahn, H. Schuitemaker, J. S. McLellan, J. P. M. Langedijk, A highly stable prefusion RSV F vaccine derived from structural analysis of the fusion mechanism. *Nat. Commun.* **6**, 8143 (2015).
12. C.-L. Hsieh, S. A. Rush, C. Palomo, C.-W. Chou, W. Pickens, V. Más, J. S. McLellan, Structure-based design of prefusion-stabilized human metapneumovirus fusion proteins. *Nat. Commun.* **13**, 1299 (2022).
13. J. S. McLellan, M. Chen, M. G. Joyce, M. Sastry, G. B. E. Stewart-Jones, Y. Yang, B. Zhang, L. Chen, S. Srivatsan, A. Zheng, T. Zhou, K. W. Graepel, A. Kumar, S. Moin, J. C. Boyington, G.-Y. Chuang, C. Soto, U. Baxa, A. Q. Bakker, H. Spits, T. Beaumont, Z. Zheng, N. Xia, S.-Y. Ko, J.-P. Todd, S. Rao, B. S. Graham, P. D. Kwong, Structure-based design of a fusion glycoprotein vaccine for respiratory syncytial virus. *Science* **342**, 592–598 (2013).
14. J. O. Ngwuta, M. Chen, K. Modjarrad, M. G. Joyce, M. Kanekiyo, A. Kumar, H. M. Yassine, S. M. Moin, A. M. Killikelly, G.-Y. Chuang, A. Druz, I. S. Georgiev, E. J. Rundlet, M. Sastry, G. B. E. Stewart-Jones, Y. Yang, B. Zhang, M. C. Nason, C. Capella, M. E. Peeples, J. E. Ledgerwood, J. S. McLellan, P. D. Kwong, B. S. Graham, Prefusion F–specific antibodies determine the magnitude of RSV neutralizing activity in human sera. *Sci. Transl. Med.* **7**, 309ra162 (2015).
15. M. S. A. Gilman, C. A. Castellanos, M. Chen, J. O. Ngwuta, E. Goodwin, S. M. Moin, V. Mas, J. A. Melero, P. F. Wright, B. S. Graham, J. S. McLellan, L. M. Walker, Rapid profiling of RSV antibody repertoires from the memory B cells of naturally infected adult donors. *Sci. Immunol.* **1**, eaaj1879 (2016).
16. E. A. F. Simões, E. Forleo-Neto, G. P. Geba, M. Kamal, F. Yang, H. Cicirello, M. R. Houghton, R. Rideman, Q. Zhao, S. L. Benvin, A. Hawes, E. D. Fuller, E. Wloga, J. M. N. Pizarro, F. M. Munoz, S. A. Rush, J. S. McLellan, L. Lipsich, N. Stahl, G. D. Yancopoulos, D. M. Weinreich, C. A. Kyratsous, S. Sivapalasingam, Suptavumab for the prevention of medically attended respiratory syncytial virus infection in preterm infants. *Clin. Infect. Dis.* **73**, e4400–e4408 (2021).
17. Q. Zhu, B. Lu, P. McTamney, S. Palaszynski, S. Diallo, K. Ren, N. D. Ulbrandt, N. Kallewaard, W. Wang, F. Fernandes, S. Wong, C. Svabek, B. Moldt, M. T. Esser, H. Jing, J. A. Suzich, Prevalence and significance of substitutions in the fusion protein of respiratory syncytial virus resulting in neutralization escape from antibody MEDI8897. *J. Infect. Dis.* **218**, 572–580 (2018).
18. X. Wen, N. Suryadevara, N. Kose, J. Liu, X. Zhan, L. S. Handal, L. E. Williamson, A. Trivette, R. H. Carnahan, T. S. Jardetzky, J. E. Crowe, Potent cross-neutralization of respiratory syncytial virus and human metapneumovirus through a structurally conserved antibody recognition mode. *Cell Host Microbe* **31**, 1288–1300.e6 (2023).
19. X. Xiao, A. Tang, K. S. Cox, Z. Wen, C. Callahan, N. L. Sullivan, D. D. Nahas, S. Cosmi, J. D. Galli, M. Minnier, D. Verma, K. Babaoglu, H. Su, A. J. Bett, K. A. Vora, Z. Chen, L. Zhang, Characterization of potent RSV neutralizing antibodies isolated from human memory B cells and identification of diverse RSV/hMPV cross-neutralizing epitopes. *MAbs* **11**, 1415–1427 (2019).
20. J. S. McLellan, M. Chen, J.-S. Chang, Y. Yang, A. Kim, B. S. Graham, P. D. Kwong, Structure of a major antigenic site on the respiratory syncytial virus fusion glycoprotein in complex with neutralizing antibody 101F. *J. Virol.* **84**, 12236–12244 (2010).
21. The IMpact-RSV Study Group, Palivizumab, a humanized respiratory syncytial virus monoclonal antibody, reduces hospitalization from respiratory syncytial virus infection in high-risk infants. *Pediatrics* **102**, 531–537 (1998).
22. C.-F. Yang, C. K. Wang, S. J. Tollefson, R. Piyaratna, L. D. Lintao, M. Chu, A. Liem, M. Mark, R. R. Spaete, J. E. Crowe, J. V. Williams, Genetic diversity and evolution of human metapneumovirus fusion protein over twenty years. *Virol. J.* **6**, 138 (2009).
23. J.-M. Yu, Y.-H. Fu, X.-L. Peng, Y.-P. Zheng, J.-S. He, Genetic diversity and molecular evolution of human respiratory syncytial virus A and B. *Sci. Rep.* **11**, 12941 (2021).
24. L. Jelley, J. Douglas, M. O'Neill, K. Berquist, A. Claasen, J. Wang, S. Utekar, H. Johnston, J. Bocacao, M. Allais, J. de Ligt, C. E. Tan, R. Seeds, T. Wood, N. Aminisani, T. Jennings, D. Welch, N. Turner, P. McIntyre, T. Dowell, A. Trenholme, C. Byrnes, SHIVERS investigation team, P. Thomas, R. Webby, N. French, Q. S. Huang, D. Winter, J. L. Geoghegan, Spatial and temporal transmission dynamics of respiratory syncytial virus in New Zealand before and after the COVID-19 pandemic. *Nat. Commun.* **15**, 9758 (2024).
25. C. A. L. Simonich, T. E. McMahon, X. Ju, T. C. Yu, N. Brunette, T. Stevens-Ayers, M. J. Boeckh, N. P. King, A. L. Greninger, J. D. Bloom, RSV F evolution escapes some monoclonal antibodies but does not strongly erode neutralization by human polyclonal sera. *J. Virol.* **99**, e00531-25 (2025).
26. N. A. Raharinirina, N. Gubela, D. Börnigen, M. R. Smith, D.-Y. Oh, M. Budt, C. Mache, C. Schillings, S. Fuchs, R. Dürrwald, T. Wolff, M. Hölzer, S. Paraskevopoulou, M. von Kleist, SARS-CoV-2 evolution on a dynamic immune landscape. *Nature* **639**, 196–204 (2025).
27. Q. Zhu, J. S. McLellan, N. L. Kallewaard, N. D. Ulbrandt, S. Palaszynski, J. Zhang, B. Moldt, A. Khan, C. Svabek, J. M. McAuliffe, D. Wrapp, N. K. Patel, K. E. Cook, B. W. M. Richter, P. C. Ryan, A. Q. Yuan, J. A. Suzich, A highly potent extended half-life antibody as a potential RSV vaccine surrogate for all infants. *Sci. Transl. Med.* **9**, eaaj1928 (2017).
28. Y. Sun, L. Liu, H. Qiang, H. Sun, Y. Jiang, L. Ren, Z. Jiang, S. Lei, L. Chen, Y. Wang, X. Lin, G. Wang, Y. Huang, Y. Fu, Y. Shi, X. Chen, H. Yu, S. Li, W. Luo, E. Liu, Q. Zheng, Z. Zheng, N. Xia, A potent broad-spectrum neutralizing antibody targeting a conserved region of the prefusion RSV F protein. *Nat. Commun.* **15**, 10085 (2024).
29. B. Ahani, K. M. Tuffy, A. A. Aksyuk, D. Wilkins, M. E. Abram, R. Dagan, J. B. Domachowske, J. D. Guest, H. Ji, A. Kushnir, A. Leach, S. A. Madhi, V. S. Mankad, E. A. F. Simões, B. Sparklin, S. D. Speer, A. M. Stanley, D. E. Tabor, U. W. Hamrén, E. J. Kelly, T. Villafana, Molecular and phenotypic characteristics of RSV infections in infants during two nirsevimab randomized clinical trials. *Nat. Commun.* **14**, 4347 (2023).
30. S. C. J. Jorgensen, Nirsevimab: Review of pharmacology, antiviral activity and emerging clinical experience for respiratory syncytial virus infection in infants. *J. Antimicrob. Chemother.* **78**, 1143–1149 (2023).
31. G.-L. Lin, S. B. Drysdale, M. D. Snape, D. O'Connor, A. Brown, G. MacIntyre-Cockett, E. Mellado-Gomez, M. de Cesare, D. Bonsall, M. A. Ansari, D. Öner, J. Aerssens, C. Butler, L. Bont, P. Openshaw, F. Martinón-Torres, H. Nair, R. Bowden, RESCEU Investigators, T. Golubchik, A. J. Pollard, Distinct patterns of within-host virus populations between two subgroups of human respiratory syncytial virus. *Nat. Commun.* **12**, 5125 (2021).
32. D. Corti, S. Bianchi, F. Vanzetta, A. Minola, L. Perez, G. Agatic, B. Guarino, C. Silacci, J. Marcandalli, B. J. Marsland, A. Piralla, E. Percivalle, F. Sallusto, F. Baldanti, A. Lanzavecchia, Cross-neutralization of four paramyxoviruses by a human monoclonal antibody. *Nature* **501**, 439–443 (2013).
33. M. Cabán, J. V. Rodarte, M. Bibby, M. D. Gray, J. J. Taylor, M. Pancera, J. Boonyaratanakornkit, Cross-protective antibodies against common endemic respiratory viruses. *Nat. Commun.* **14**, 798 (2023).
34. E. Goodwin, M. S. A. Gilman, D. Wrapp, M. Chen, J. O. Ngwuta, S. M. Moin, P. Bai, A. Sivasubramanian, R. I. Connor, P. F. Wright, B. S. Graham, J. S. McLellan, L. M. Walker, Infants infected with respiratory syncytial virus generate potent neutralizing antibodies that lack somatic hypermutation. *Immunity* **48**, 339–349.e5 (2018).
35. F. Frank, M. M. Keen, A. Rao, L. Bassit, X. Liu, H. B. Bowers, A. B. Patel, M. L. Cato, J. A. Sullivan, M. Greenleaf, A. Piantadosi, W. A. Lam, W. H. Hudson, E. A. Ortlund, Deep mutational scanning identifies SARS-CoV-2 Nucleocapsid escape mutations of currently available rapid antigen tests. *Cell* **185**, 3603–3616.e13 (2022).
36. Z. Cui, P. Liu, N. Wang, L. Wang, K. Fan, Q. Zhu, K. Wang, R. Chen, R. Feng, Z. Jia, M. Yang, G. Xu, B. Zhu, W. Fu, T. Chu, L. Feng, Y. Wang, X. Pei, P. Yang, X. S. Xie, L. Cao, Y. Cao, X. Wang, Structural and functional characterizations of infectivity and immune evasion of SARS-CoV-2 Omicron. *Cell* **185**, 860–871.e13 (2022).
37. A. J. Greaney, T. N. Starr, P. Gilchuk, S. J. Zost, E. Binshtein, A. N. Loes, S. K. Hilton, J. Huddleston, R. Eguia, K. H. D. Crawford, A. S. Dingens, R. S. Nargi, R. E. Sutton, N. Suryadevara, P. W. Rothlauf, Z. Liu, S. P. J. Whelan, R. H. Carnahan, J. E. Crowe Jr., J. D. Bloom, Complete mapping of mutations to the SARS-CoV-2 spike receptor-binding domain that escape antibody recognition. *Cell Host Microbe* **29**, 44–57.e9 (2021).
38. T. N. Starr, A. J. Greaney, S. K. Hilton, D. Ellis, K. H. D. Crawford, A. S. Dingens, M. J. Navarro, J. E. Bowen, M. A. Tortorici, A. C. Walls, N. P. King, D. Veesler, J. D. Bloom, Deep mutational scanning of SARS-CoV-2 receptor binding domain reveals constraints on folding and ACE2 binding. *Cell* **182**, 1295–1310.e20 (2020).
39. Y. Cao, A. Yisimayi, F. Jian, W. Song, T. Xiao, L. Wang, S. Du, J. Wang, Q. Li, X. Chen, Y. Yu, P. Wang, Z. Zhang, P. Liu, R. An, X. Hao, Y. Wang, J. Wang, R. Feng, H. Sun, L. Zhao, W. Zhang, D. Zhao, J. Zheng, L. Yu, C. Li, N. Zhang, R. Wang, X. Niu, S. Yang, X. Song, Y. Chai, Y. Hu, Y. Shi, L. Zheng, Z. Li, Q. Gu, F. Shao, W. Huang, R. Jin, Z. Shen, Y. Wang, X. Wang, J. Xiao, X. S. Xie, BA.2.12.1, BA.4 and BA.5 escape antibodies elicited by Omicron infection. *Nature* **608**, 593–602 (2022).
40. J. S. McLellan, M. Chen, S. Leung, K. W. Graepel, X. Du, Y. Yang, T. Zhou, U. Baxa, E. Yasuda, T. Beaumont, A. Kumar, K. Modjarrad, Z. Zheng, M. Zhao, N. Xia, P. D. Kwong, B. S. Graham, Structure of RSV fusion glycoprotein trimer bound to a prefusion-specific neutralizing antibody. *Science* **340**, 1113–1117 (2013).
41. A. Tang, Z. Chen, K. S. Cox, H.-P. Su, C. Callahan, A. Fridman, L. Zhang, S. B. Patel, P. J. Cejas, R. Swoyer, S. Touch, M. P. Citron, D. Govindarajan, B. Luo, M. Eddins, J. C. Reid, S. M. Soisson, J. Galli, D. Wang, Z. Wen, G. J. Heidecker, D. R. Casimiro, D. J. DiStefano, K. A. Vora, A potent broadly neutralizing human RSV antibody targets conserved site IV of the fusion glycoprotein. *Nat. Commun.* **10**, 4153 (2019).
42. J. Zikherman, GC B cells 'AKT' to blunt BCR signaling. *Nat. Immunol.* **20**, 671–674 (2019).
43. Y. Cao, F. Jian, Z. Zhang, A. Yisimayi, X. Hao, L. Bao, F. Yuan, Y. Yu, S. Du, J. Wang, T. Xiao, W. Song, Y. Zhang, P. Liu, R. An, P. Wang, Y. Wang, S. Yang, X. Niu, Y. Zhang, Q. Gu, F. Shao, Y. Hu, W. Yin, A. Zheng, Y. Wang, C. Qin, R. Jin, J. Xiao, X. S. Xie, Rational identification of

potent and broad sarbecovirus-neutralizing antibody cocktails from SARS convalescents. *Cell Rep.* **41**, 111845 (2022).
44. Y. Li, J. Wang, C. Zhang, Y. Zhang, J. Deng, H. Zhang, M. Li, F. Wang, X. Wang, MAAD: Multidimensional Antiviral Antibody Database. *Protein Cell*, https://doi.org/10.1093/procel/pwaf106 (2025).
45. C. G. Rappazzo, C.-L. Hsieh, S. A. Rush, E. S. Esterman, T. Delgado, J. C. Geoghegan, A. Z. Wec, M. Sakharkar, V. Más, J. S. McLellan, L. M. Walker, Potently neutralizing and protective anti-human metapneumovirus antibodies target diverse sites on the fusion glycoprotein. *Immunity* **55**, 1710–1724.e8 (2022).
46. K. Wang, Z. Jia, L. Bao, L. Wang, L. Cao, H. Chi, Y. Hu, Q. Li, Y. Zhou, Y. Jiang, Q. Zhu, Y. Deng, P. Liu, N. Wang, L. Wang, M. Liu, Y. Li, B. Zhu, K. Fan, W. Fu, P. Yang, X. Pei, Z. Cui, L. Qin, P. Ge, J. Wu, S. Liu, Y. Chen, W. Huang, Q. Wang, C.-F. Qin, Y. Wang, C. Qin, X. Wang, Memory B cell repertoire from triple vaccinees against diverse SARS-CoV-2 variants. *Nature* **603**, 919–925 (2022).
47. Y. Cao, B. Su, X. Guo, W. Sun, Y. Deng, L. Bao, Q. Zhu, X. Zhang, Y. Zheng, C. Geng, X. Chai, R. He, X. Li, Q. Lv, H. Zhu, W. Deng, Y. Xu, Y. Wang, L. Qiao, Y. Tan, L. Song, G. Wang, X. Du, N. Gao, J. Liu, J. Xiao, X.-D. Su, Z. Du, Y. Feng, C. Qin, C. Qin, R. Jin, X. S. Xie, Potent neutralizing antibodies against SARS-CoV-2 identified by high-throughput single-cell sequencing of convalescent patients' B cells. *Cell* **182**, 73–84.e16 (2020).
48. C. J. Knudson, S. M. Hartwig, D. K. Meyerholz, S. M. Varga, RSV vaccine-enhanced disease is orchestrated by the combined actions of distinct CD4 T cell subsets. *PLOS Pathogens* **11**, e1004757 (2015).
49. T. Jenkins, R. Wang, O. Harder, M. Xue, P. Chen, J. Corry, C. Walker, M. Teng, A. Mejias, O. Ramilo, S. Niewiesk, J. Li, M. E. Peeples, A novel live attenuated respiratory syncytial virus vaccine candidate with mutations in the L protein SAM binding site and the G protein cleavage site is protective in cotton rats and a rhesus macaque. *J. Virol.* **95**, e01568-20 (2021).
50. Y. Cao, J. Wang, F. Jian, T. Xiao, W. Song, A. Yisimayi, W. Huang, Q. Li, P. Wang, R. An, J. Wang, Y. Wang, X. Niu, S. Yang, H. Liang, H. Sun, T. Li, Y. Yu, Q. Cui, S. Liu, X. Yang, S. Du, Z. Zhang, X. Hao, F. Shao, R. Jin, X. Wang, J. Xiao, Y. Wang, X. S. Xie, Omicron escapes the majority of existing SARS-CoV-2 neutralizing antibodies. *Nature* **602**, 657–663 (2022).
51. A. Punjani, J. L. Rubinstein, D. J. Fleet, M. A. Brubaker, cryoSPARC: Algorithms for rapid unsupervised cryo-EM structure determination. *Nat. Methods* **14**, 290–296 (2017).
52. K. Tunyasuvunakool, J. Adler, Z. Wu, T. Green, M. Zielinski, A. Žídek, A. Bridgland, A. Cowie, C. Meyer, A. Laydon, S. Velankar, G. J. Kleywegt, A. Bateman, R. Evans, A. Pritzel, M. Figurnov, O. Ronneberger, R. Bates, S. A. A. Kohl, A. Potapenko, A. J. Ballard, B. Romera-Paredes, S. Nikolov, R. Jain, E. Clancy, D. Reiman, S. Petersen, A. W. Senior, K. Kavukcuoglu, E. Birney, P. Kohli, J. Jumper, D. Hassabis, Highly accurate protein structure prediction for the human proteome. *Nature* **596**, 590–596 (2021).
53. E. F. Pettersen, T. D. Goddard, C. C. Huang, E. Meng, G. S. Couch, T. I. Croll, J. H. Morris, T. E. Ferrin, UCSF ChimeraX: Structure visualization for researchers, educators, and developers. *Protein Sci.* **30**, 70–82 (2020).
54. P. Emsley, K. Cowtan, Coot: Model-building tools for molecular graphics. *Acta Crystallogr. D Biol. Crystallogr.* **60**, 2126–2132 (2004).
55. P. V. Afonine, B. P. Klaholz, N. W. Moriarty, B. K. Poon, O. V. Sobolev, T. C. Terwilliger, P. D. Adams, A. Urzhumtsev, New tools for the analysis and validation of cryo-EM maps and atomic models. *Acta Crystallogr. D Struct. Biol.* **74**, 814–840 (2018).

Acknowledgments: We thank X. Huang, X. Li, B. Zhu, and L. Chen for cryo-EM data collection at the Center for Biological Imaging (CBI), Institute of Biophysics. We thank Y. Chen, Z. Yang, and B. Zhou for technical support on BLI. We sincerely thank all pediatric health care workers from the Children's Hospital of Chongqing Medical University who contributed blood samples for this study. We are grateful to Vazyme Biotech Co., Ltd. for their assistance with RSV F–specific memory B cell sorting and sequencing. **Funding:** This work was supported by the Strategic Priority Research Program (XDB1310000, X.W.); National Science and Technology Major Project (2025ZD01903800, X.W.); National Science Foundation grants (32325004, T2394482, and 12034006, X.W.); Basic Research Program Based on Major Scientific Infrastructures, CAS-JZHKYPT-2021-05, CAS (YSBR-010, X.W.); National Key Research and Development Program (2023YFC2306003, X.W.); Ministry of Science and Technology of China (CPL-1233, X.W.); National Key Research and Development Program (2022YFC2704900, E.L.); and Chongqing Talent Plan Innovation and Entrepreneurship Team (2022, E.L.). This work has been supported by the New Cornerstone Science Foundation (X.W.). **Author contributions:** X.W., E.L., Y.C., and L.R. designed and supervised the study. X.W. and H.Z. wrote the manuscript. H.Z. designed and performed the in vitro and in vivo studies and analyzed the data. W.Y. solved atomic structures and performed visualization for data in this study. J.W. analyzed the prevalence of RSV or hMPV strains. J.D. analyzed the interaction between antigens and antibodies. Under the supervision of Y.C., S.L. conducted a detailed analysis of antibody escape from binding by performing DMS. T.Z. performed the neutralization of mAbs against RSV isolates. Y.L. analyzed amino acid sequences of the mAbs. K.X. collected cryo-EM data related to CNR2056 and CNR2047. M.M. and R.F. purified the pre-F of RSV and hMPV. Y.H. provided guidance on evaluating the protective efficacy of the mAbs in vivo. H.Z. and L.R. collected the blood samples and clinical specimens. All authors reviewed and approved the final manuscript. **Competing interests:** X.W., R.F., H.Z., W.Y., J.W., and J.D. are listed as inventors of Chinese patent applications for RSV F–specific antibodies involved in CNR2047 and CNR2056 (an antibody or antigen-binding fragment against RSV and hMPV and their applications, 202410173682.X). H.Z., E.L., X.W., L.R., J.D., W.Y., R.F., and Y.L. are listed as inventors of Chinese patent applications for CNR2053 (antibody specifically binding to RSV and its applications, 202511484940.7). The other authors declare that they have no competing interests. **Data, code, and materials availability:** All data associated with this study are present in the paper or the Supplementary Materials. The cryo-EM density maps and corresponding atomic models have been deposited in the Electron Microscopy Data Bank (EMDB; http://www.ebi.ac.uk/pdbe/emdb/) and Protein Data Bank (PDB; https://www.ebi.ac.uk/pdbe), respectively. The accession codes are available for the RSV pre-F complex with CNR2042 (EMDB: EMD-64666, PDB: 9V0N), RSV pre-F complex with CNR2047 (EMDB: EMD-64670, PDB: 9V0S), RSV pre-F complex with CNR2053 (EMDB: EMD-64667, PDB: 9V0P), RSV pre-F complex with CNR2056 (EMDB: EMD-64668, PDB: 9V0Q), hMPV pre-F complex with CNR2047 (EMDB: EMD-64671, PDB: 9V0T), RSV pre-F monomer complex with CNR2056 and CNR2047 (EMDB: EMD-64735, PDB: 9V2O), RSV pre-F dimer complex with CNR2056 and CNR2047 (EMDB: EMD-64737, PDB: 9V2Q), and RSV pre-F trimer complex with CNR2056/CNR2047 (EMDB: EMD-64738, PDB: 9V2R). Detailed antibody data have been deposited to the Multidimensional Antiviral Antibody Database (MAAD) (*44*), and the DMS data are also available online at https://doi.org/10.5281/zenodo.17952000. Custom scripts and processed data for the DMS analysis are available online at https://doi.org/10.5281/zenodo.18150586. All materials used or generated in this study are commercially available or will be supplied upon reasonable request.

Submitted 6 June 2025
Accepted 8 January 2026
Published 18 February 2026
10.1126/scitranslmed.adz4170

Science Translational Medicine

Antibody cocktails based on the occupationally acquired immunity of pediatricians neutralize and confer protection against RSV and hMPV

Hui Zhai, Wenxiang Yu, Jinyue Wang, Jie Deng, Siyu Lei, Teng Zhou, Yixin Li, Kaijun Xu, Mengyang Ma, Rui Feng, Yaling Hu, Luo Ren, Yunlong Cao, Enmei Liu, and Xiangxi Wang

Sci. Transl. Med. **18** (837), eadz4170. DOI: 10.1126/scitranslmed.adz4170

Editor's summary

Pediatricians are routinely exposed to respiratory viruses such as respiratory syncytial virus (RSV) and human metapneumovirus (hMPV); as such, their immune systems may offer a distinctly mature source of antibodies capable of neutralizing these viruses. Here, Zhai *et al.* isolated B cells from pediatricians, then characterized monoclonal antibodies (mAbs) produced by those B cells. The authors identified several mAbs targeting sites Ø and III on the pre–fusion protein that could potently neutralize RSV and hMPV, including CNR2047, which neutralized both. The authors showed that monotherapy with the identified mAbs conferred protection against RSV and hMPV infection in preclinical models. The mAbs performed even better when rationally combined into a cocktail targeting both sites Ø and III. Together, these data support further development of these rationally designed mAb cocktails for RSV and hMPV prevention. —Courtney Malo